Mice with renal-specific alterations of stem cell-associated signaling develop symptoms of chronic kidney disease but surprisingly no tumors

Stem cell-associated signaling in the kidney

Adam Myszczyszyn[1,*], Oliver Popp[2], Severine Kunz[3], Anje Sporbert[4], Simone Jung[1], Louis C. Penning[5], Annika Fendler[1], Philipp Mertins[2,6], Walter Birchmeier[1,6]

1 Cancer Research Program, Max Delbrueck Center for Molecular Medicine (MDC) in the Helmholtz Association, Robert-Roessle-Strasse 10, 13125 Berlin, Germany

2 Proteomics, Max Delbrueck Center for Molecular Medicine (MDC) in the Helmholtz Association, Robert-Roessle-Strasse 10, 13125 Berlin, Germany

3 Electron Microscopy, Max Delbrueck Center for Molecular Medicine (MDC) in the Helmholtz Association, Robert-Roessle-Strasse 10, 13125 Berlin, Germany

4 Advanced Light Microscopy, Max Delbrueck Center for Molecular Medicine (MDC) in the Helmholtz Association, Robert-Roessle-Strasse 10, 13125 Berlin, Germany

5 Faculty of Veterinary Medicine, Utrecht University, Yalelaan 1, 3584 CL Utrecht, The Netherlands

6 Senior author

** Corresponding author: adam.myszczyszyn@gmail.com*

Abstract

Previously, we found that Wnt and Notch signaling govern stem cells of clear cell kidney cancer (ccRCC) in patients. To mimic stem cell responses in the normal kidney in vitro in a marker-unbiased fashion, we have established organoids from total single adult mouse kidney epithelial cells in Matrigel and serum-free conditions. Deep proteomic and phosphoproteomic analyses revealed that the organoids resembled renewal of adult kidney tubular epithelia, since organoid cells displayed activity of Wnt and Notch signaling, long-term proliferation and expression of markers of proximal and distal nephron lineages. In our wish to model stem cell-derived human ccRCC, we have generated two types of genetic double kidney mutants in mice: Wnt-β-catenin-GOF together with Notch-GOF and Wnt-β-catenin-GOF together with a most common alteration in ccRCC, Vhl-LOF. An inducible Pax8-rtTA-LC1-Cre was used to drive recombination specifically in adult kidney epithelial cells. We confirmed mutagenesis of β-catenin, Notch and Vhl alleles on DNA, protein and mRNA target gene levels. Surprisingly, we observed symptoms of chronic kidney disease (CKD) in mutant mice, but no increased proliferation and tumorigenesis. Thus, the responses of kidney stem cells in the organoid and genetic systems produced different phenotypes, i.e. enhanced renewal versus CKD.

Introduction

Over the past few decades, Wnt-β-catenin and Notch have emerged as fundamental signal transduction systems, which regulate maintenance and differentiation of stem cells in homeostasis and regeneration of adult organs (1,2). In the mouse kidney, Wnt and Notch signaling are upregulated in Sox9-positive progenitors that contribute to regeneration of proximal tubule, Loop of Henle and distal tubule (3). Unipotent progenitors specific for proximal, distal and collecting duct segments were reported in *Rainbow* mice, which drive homeostatic maintenance and regeneration of the kidney and are Wnt-responsive (4). Moreover, deletion of the Wnt mediator β-catenin in kidney tubular cells and blocking Notch with a γ-secretase inhibitor delayed kidney recovery upon injury in mice (5,6). Together, activity of Wnt and Notch signaling seems to be a common feature of different kidney stem/progenitor cell populations.

Organoids are emerging as powerful tools to study properties of stem/progenitor cells in adult epithelial tissues. Organoids are 3D structures grown from stem/progenitor cells in culture with Matrigel and well-defined growth factors. During organoid formation, cells self-renew, differentiate and self-organize by cell sorting and spatially restricted lineage commitment in a manner similar to natural organs. Thus, organoids recapitulate stem/progenitor cell behaviors during homeostatic maintenance and regeneration of adult epithelia (7,8). Adult kidney organoids were created from normal human and mouse kidneys (9,10). However, characterization of stemness in these organoids has not been pushed forward to a satisfying level.

Clear cell renal cell carcinoma (ccRCC) is the most frequent and aggressive human kidney cancer (11). Inactivation of the Von Hippel-Lindau (*VHL*) tumor suppressor gene followed by a HIF-1α- and HIF-2α-mediated hypoxic state occurs in the majority of ccRCC cases (12). However, deletion of Vhl in mouse kidneys is insufficient for tumorigenesis (13). Our laboratory identified CXCR4-, MET- and CD44-enriched cancer stem cells (CSCs) in human ccRCCs

67 (14). The CSCs displayed upregulation of Wnt and Notch signaling and quantitatively
68 correlated with advanced stages, aggressiveness and metastasis of tumors. Treatment with
69 small-molecule inhibitors of Wnt and Notch blocked self-renewal of the CSCs in patient-derived
70 models, i.e. in subcutaneous and orthotopic xenografts, and in organoids and non-adherent
71 spheres in cultures. This points to a crucial role of Wnt-high and Notch-high stem/progenitor
72 cells as actors in kidney tumorigenesis.
73
74 Upregulation of Wnt signaling in combination with genetic interferences at p53 or p21 in mouse
75 kidneys using embryonic Cres was sufficient to overcome Wnt-induced p53-p21-mediated
76 senescence and resulted in development of malignant lesions that displayed characteristics of
77 non-ccRCCs (15,16). Concomitant upregulation of Wnt and K-ras signaling in embryonic
78 mouse kidneys also drove formation of malignant lesions that resembled non-ccRCCs,
79 including pediatric tumors (17,18). Hyperactivation of Notch signaling in combination with Vhl
80 loss in adult mouse kidneys contributed to development of premalignant lesions with some
81 hallmarks of ccRCC (19,20). However, upregulation of either Wnt or Notch in adult Cd133-
82 positive kidney cells in mice failed to produce tumors (21). Answer to a fundamental question
83 remains elusive on whether the functional interplay of Wnt and Notch drives tumorigenesis in
84 the kidney, also in the context of Vhl inactivation.
85
86 To reveal the importance of Wnt and Notch signaling for adult renal stem/progenitor cells in
87 vitro without enriching populations positive for a specific marker, we have established tubular
88 organoids from whole mouse kidneys in Matrigel in serum-free conditions. Then, to mimic
89 development of human ccRCC from Wnt- and Notch-dependent stem cells, we have generated
90 genetic mutants in mice, i.e. Wnt-β-catenin-GOF together with Notch-GOF or with Vhl-LOF,
91 using an adult kidney tubular epithelium-specific Cre to circumvent embryonic or postnatal
92 kidney defects and non-renal confounding influences.
93

Materials and Methods

Mice

The Landesamt für Gesundheit und Soziales (LaGeSo) in Berlin approved the mouse study (G0342/13). Mice were housed and bred in the IVC cages type II at 21°C ambient temperature, at 50-60% humidity, in a 12-h dark/light cycle and in pathogen-free conditions. LC1-Cre mice (22) were a kind gift from Klaus Rajewsky (MDC). β-catenin-loxP (23), Notch-loxP (24) and LacZ-loxP (25) mice came from in-house colonies. Pax8-rtTA B6.Cg-Tg(Pax8-rtTA2S*M2)1Koes/J (26) and Vhl-loxP B6.129S4(C)-Vhltm1Jae/J (27) mice were purchased from the Jackson Laboratory. The studies in the organoids and genetic mouse models were performed using both male and female mice of a mixed C57BL/6J and FVB/NJ background, unless otherwise stated. To establish the genetic mouse models, adult one-month-old Pax8-rtTA-LC1-Cre-loxP mice and controls carrying loxP alleles, but no Pax8-rtTA and/or LC1-Cre (both males and females) were exposed for 5 days to doxycycline (Sigma-Aldrich) at the concentration of 0.2 mg/ml in drinking water supplemented with 5% sucrose. According to a score sheet, mice were checked at least twice per week until illness symptoms were observed. Sick mice were immediately sacrificed and biological material was collected.

Preparation of kidney cell suspensions

Kidneys were harvested and transferred to MEM with Earle's Salts (with 2.2 g/l NaHCO3, without L-Glutamine) medium (Biochrom) supplemented with 10% FCS (Life Technologies), 1x Non-Essential Amino Acids (NEAA, Thermo Fisher Scientific), 2 mM L-Glutamine (Biochrom), 1x Penicillin-Streptomycin (Life Technologies) and 125 µg/ml Amphotericin B (Biomol). Whole kidneys were minced into pieces smaller than 1 mm3, digested in 2 mg/ml Collagenase P (Roche) for 45 min and filtered through sieves with 70 and 40 µm pore size. Erythrocytes were lysed in RBC lysis buffer and lymphocytes were depleted by MACS using CD45 microbeads (Miltenyi Biotec) according to the manufacturer's instructions.

121 **Kidney organoid cultures**

122 Freshly isolated cell suspensions were seeded at 10^5 cells per well in 25 µl Matrigel (75%,
123 Corning) lenses in 48-well plates. Matrigel drops were overlayed with 250 µl organoid medium
124 (Table 1). Medium was changed every other day. The organoids were passaged for the first
125 time after 14 days and subsequently once per week. Matrigel lenses were mechanically broken
126 and the organoids were collected and dissociated to small cell clusters using TrypLE Select
127 (Life Technologies) for 10 min. In the first two passages, collected organoids were additionally
128 filtered through a sieve with 40 µm pore size. Cultures were passaged in 1:3 ratios. If single
129 cell suspensions were needed, the organoids were dissociated in TrypLE for 1 hr. Cell clusters
130 from the organoids were cryopreserved at an early passage in 1 ml Recovery Cell Culture
131 Freezing Medium (Thermo Fisher Scientific) according to the manufacturer's instructions. BrdU
132 (Thermo Fisher Scientific) treatment (at 10 µM) was performed for 4 hrs prior to organoid
133 collection for staining. For functional assays, 100 ng/ml human Wnt3a (R&D Systems) was
134 added. For the examination of structural changes of the organoids upon R-spondin-1
135 withdrawal or ICG-001 treatment, single cells were seeded at 45,000 cells in 48-well plates
136 and cultured 7 days in organoid medium without R-spondin-1 or cultured 24h in normal medium
137 and 6 days in medium containing ICG-001 (Biochem-partner) at IC50. Brightfield and
138 fluorescence images were acquired with a Leica DMI 6000 B microscope using the Leica LAS
139 X software.

140

141 **Table 1. Medium components for organoid culture.**

Component	Function	Concentration	Supplier
Advanced DMEM/F12 with GlutaMax	Basal medium	–	Life Technologies
Penicillin-Streptomycin	Antibiotics	1x	Life Technologies
Amphotericin B	Antifungal	125 µg/ml	Biomol

HEPES	Buffer	10 mM	Life Technologies
N-acetylcysteine	Antioxidant	1.25 mM	Sigma-Aldrich
B27	Serum-free growth supplement	1x	Life Technologies
N2	Serum-free growth supplement	1x	Life Technologies
Nicotinamide	Increasing organoid formation and lifespan via inhibiting sirtuin activity involved in apoptosis and differentiation (28,29)	10 mM	Sigma-Aldrich
Human EGF	Stimulating proliferation, inhibiting apoptosis (28,29)	50 ng/ml	Peprotech
A83-01	Blocking differentiation and promoting long-term culture of stem cells via inhibiting TGFβ signaling (28,29)	500 nM	Sigma-Aldrich
Human R-spondin-1	Maintaining stem cells via agonizing Wnt signaling (28,29)	500 ng/ml	Peprotech
Hydrocortisone (HC)	Acting anti-inflammatory via repressing activity of NF-κB and AP-1 (30), inducing Yap signaling (31)	0.5 µg/ml	Sigma-Aldrich
Prostaglandin E2 (PGE2)	Preventing anoikis and promoting stem cell survival via enhancing Wnt signaling (28)	1 µM	Sigma-Aldrich

142

143 **Proteomics and phosphoproteomics**

144 Three independent replicates of early (OEP) and long-term (OLP) passage organoids were
145 released from Matrigel by mechanical disruption, collected in a conical tube and incubated with
146 the non-enzymatic Cell Recovery Solution (Corning) according to the manufacturer's

147 instructions to remove Matrigel rests. Three independent replicates of Epcam-positive kidney
148 epithelial cells (control kidney, CK) were MAC-sorted from freshly isolated single cell
149 suspensions from whole mouse kidneys using microbeads (Miltenyi Biotec) according to the
150 manufacturer's instructions. Global proteomic and phosphoproteomic characterization of the
151 samples was achieved by the tandem mass tag (TMT)-based quantitation using the TMT 10-
152 plex reagents (Thermo Fisher Scien-tific), as previously described (32). Briefly, samples were
153 lysed in urea lysis buffer containing protease and phosphatase inhibitors, subjected to tryptic
154 in-solution digest and labeled with the TMT 10-plex reagents. After pooling, samples were
155 separated into 24 fractions for the proteomic and 12 fractions for the phosphoproteomic
156 analysis using basic reversed-phase HPLC. Phosphopeptides were enriched from each
157 fraction using robot-assisted iron-based IMAC on an AssayMap Bravo system (Agilent).
158 Proteomic and phosphoproteomic samples were measured on a Q Exactive HF-X orbitrap
159 mass spectrometer (Thermo Fisher Scientific) connected to an EASY-nLC system (Thermo
160 Fisher Scientific) applying a 110-min online HPLC gradient. MS acquisition was performed at
161 a resolution of 60,000 in a scan range from 350 to 1500 Th. Data-dependent MS2 scans were
162 carried out at a resolution of 45,000 with an isolation window of 0.7 Th and a maximum injection
163 time of 86 ms using the top 20 peaks from each precursor scan for HCD fragmentation. For
164 the data analysis, the MaxQuant software package version 1.6.10.43 (33) was used. A FDR
165 cutoff of 0.01 was applied for peptides and proteins and database search was performed using
166 the mouse Uniprot database (July 2018), including isoforms. Variable modifications included
167 phosphorylation on serine, threonine and tyrosine, methionine-oxidation, acetylated N-termini
168 and deamidation of asparagine and glutamine, while the TMT10-plex reporter ion quantitation
169 was turned on using a PIF setting of 0.5. Log2-transformed and median-MAD centered
170 corrected reporter ion intensities were used for quantitation. Protein groups were filtered for
171 proteins, which were identified by at least one unique peptide and at least two peptides in total
172 and had valid values across all samples. Phosphorylation site tables were filtered for valid
173 values across all samples. For significance calling, a two-sample moderated t-testing (limma
174 R package) (34) was applied. A multiple comparison correction was done using the Benjamini-

175 Hochberg method (adjusted P-values). The KEGG PATHWAY (mmu04310) and a previously
176 published list (35) served as a combined reference protein list for the Wnt signaling heatmap.
177 The KEGG PATHWAY (mmu04330) served as a reference protein list for the Notch signaling
178 heatmap. A previously published list (36) served as a reference protein list for the Yap signaling
179 heatmap.
180
181 **Section staining**
182 The organoids were released from Matrigel by mechanical disruption, collected in a conical
183 tube and fixed in 10% (v/v) Neutral-buffered Formalin overnight. The organoids were
184 transferred to a 2-ml tube and overlayed with 1.5% agarose. The resulting agarose beads were
185 dehydrated and embedded in paraffin. All stainings were performed on 5-µm sections. For
186 haematoxylin-eosin (H&E) staining, sections were rehydrated and stained with haematoxylin
187 (Fluka) for 4 min and with eosin (Merck) for 2 min. For immunofluorescence, sections were
188 rehydrated, and antigen retrieval in TRIS-EDTA and blocking with 10% donkey serum (Bio-
189 Rad) were performed. Sections were incubated overnight with rat anti-BrdU (1:100, Abcam,
190 ab6326), mouse anti-E-cad (1:300, BD Biosciences, 610181), rabbit anti-Laminin (1:500,
191 Abcam, ab11575), rat anti-Zo-1 (1:200, Santa Cruz, sc-33725), mouse anti-MDR1 (1:50, Santa
192 Cruz, sc-55510) and mouse anti-AQP3 (1:50, Santa Cruz, sc-518001) primary antibodies or
193 with Biotinylated LTL (1:300, Vector Laboratories, B-1325) and Rhodamine-conjugated PNA
194 (1:300, Vector Laboratories, RL-1072) lectins, followed by incubation with donkey fluorescent
195 dye-conjugated Alexa488 anti-mouse, Alexa488 anti-rabbit, Alexa488 anti-rat and Cy3 anti-rat
196 (1:250, Jackson) secondary antibodies or with Alexa647-conjugated Streptavidin (1:200,
197 Thermo Fisher Scientific) and by counterstaining with DAPI (0.2 µg/ml, Thermo Fisher
198 Scientific) for 1 hr. For immunohistochemistry, sections were rehydrated, antigen retrieval in
199 TRIS-EDTA was performed, endogenous peroxidase activity was blocked in 3.5% (v/v)
200 hydrogen peroxide and blocking with 10% donkey serum (Bio-Rad) was performed. Sections
201 were incubated overnight with rabbit anti-Pax8 primary antibody (1:2000, Proteintech, 10336-
202 1-AP), followed by incubation with peroxidase-conjugated donkey anti-rabbit secondary

203 antibody from a kit (Dako) for 1 hr. Sections were developed using the substrate-chromogen
204 system (Dako) and counterstained with haematoxylin (Fluka) for 2 min. Kidneys and spleens
205 were fixed in 10% (v/v) Neutral-buffered Formalin overnight, dehydrated and embedded in
206 paraffin. All stainings were performed on 5 µm sections. For immunohistochemistry, sections
207 were rehydrated, antigen retrieval in TRIS-EDTA was performed, endogenous peroxidase
208 activity was blocked in 3.5% (v/v) hydrogen peroxide and blocking with 10% donkey serum
209 (Bio-Rad) was performed. Sections were incubated overnight with rabbit anti-N1icd (1:100,
210 Cell Signaling, 4147S), rabbit anti-Ki67 (1:200, Thermo Fisher Scientific, RM-9106-S), mouse
211 anti-phospho-γH2AX (1:500, Merck Millipore, 05-636), mouse anti-p53 (1:100, Santa Cruz, sc-
212 126) and mouse anti-p21 (1:100, Santa Cruz, sc-6246) primary antibodies, followed by
213 incubation with peroxidase-conjugated donkey anti-rabbit and anti-mouse secondary
214 antibodies from a kit (Dako) for 1 hr. Sections were developed using the substrate-chromogen
215 system (Dako) and counterstained with haematoxylin (Fluka) for 2 min. For PAS staining,
216 sections were rehydrated, stained using the Periodic Acid-Schiff (PAS) Kit (Sigma-Aldrich)
217 according to the manufacturer's instructions and counterstained with haematoxylin (Fluka) for
218 2 min. For LacZ staining, cryosections were prepared. Kidneys were placed in 30% sucrose in
219 PBS overnight and embedded in OCT compound (Sakura Finetek). 10-µm sections were fixed
220 in 0.2% (v/v) glutaraldehyde for 10 min, washed three times in washing solution (PBS, 2 mM
221 MgCl2, 0.01% sodium deoxycholate and 0.02% NP-40), incubated overnight in staining
222 solution (PBS, 2 mM MgCl2, 0.01% sodium deoxycholate, 0.02% NP-40, 5 mM K3Fe(CN)6,
223 5 mM K4Fe(CN)6 and 1 mg/ml X-gal (Roth)) and counterstained with nuclear fast red (Merck)
224 for 5 min. Images were taken with an Axio Imager.Z1 microscope (for immunofluorescence) or
225 an Axio Scope.A1 microscope (for H&E staining, PAS staining, LacZ staining and
226 immunohistochemistry) using the Zen software (all Zeiss). Selected immunofluorescence
227 images were processed with Fiji ImageJ.
228
229 **Whole mount staining**

230 The organoids were released from Matrigel by mechanical disruption, collected, transferred to
231 a 2-ml tube, fixed in 10% (v/v) Neutral-buffered Formalin for 1.5 hrs and blocked in 10% donkey
232 serum (Bio-Rad) for 2 hrs. The organoids were incubated overnight with mouse anti-E-cad
233 primary antibody (1:300, BD Biosciences, 610181), Biotinylated LTL lectin (1:300, Vector
234 Laboratories, B-1325) and Rhodamine-conjugated PNA lectin (1:300, Vector Laboratories, RL-
235 1072), and then overnight with donkey Alexa488 anti-mouse secondary antibody (1:250,
236 Jackson), Alexa647-conjugated Streptavidin (1:200, Thermo Fisher Scientific) and DAPI (0.2
237 µg/ml, Thermo Fisher Scientific). The organoids were taken up in 1.5% low-melting agarose
238 and transferred to chamber slides. Confocal z-stacks were acquired with a LSM700 or LSM710
239 microscope (Zeiss) using a long working distance C-Achroplan 32x/0.85 water immersion
240 objective and Immersol W (Zeiss). DAPI, Alexa488, Cy3 and Alexa647 fluorophores were
241 excited with a 405 nm, 488 nm, 561 nm and 633 nm laser, respectively, and detected by
242 sequential scanning using BP filters 410-460 nm, 500-540 nm, 565-620 nm and 640-720 nm,
243 respectively. Images were acquired with a pixel size of 0.116 or 0.142 µm (lateral) and 1.11 or
244 1.16 µm (axial) with 12-bit and line average 2. If necessary, detector gain and laser power
245 were slightly adjusted with z-depth to keep a constant signal. Restoration of confocal z-stacks
246 was performed with the Huygens Deconvolution software (SVI) running on a dedicated data
247 processing workstation (Acquifer) using a CMLE algorithm with 60 iterations and a SNR of 12.
248 After deconvolution, confocal z-stacks were 3D reconstructed using the Imaris 9.1 software
249 (Bitplane/Oxford Instruments) and either the volume reconstruction and clipping planes or
250 orthogonal sections were used to visualize and explore the 3D structure of the organoids.
251

252 **Transmission electron microscopy**

253 The organoids were released from Matrigel by mechanical disruption, collected in a conical
254 tube and fixed in 2% (w/v) formaldehyde and 2.5% (v/v) glutaraldehyde in 0.1 M phosphate
255 buffer for 2 hrs. After embedding in 10% agarose in a 2-ml tube, samples were post-fixed with
256 1% (v/v) osmium tetroxide (Sigma-Aldrich), dehydrated in a graded series of EtOH and
257 embedded in PolyBed® 812 resin (Polysciences). Ultrathin sections (60-80 nm) were stained

258 with uranyl acetate (Polysciences) and lead citrate (Sigma-Aldrich) and examined at 80 kV
259 with an EM 910 electron microscope (Zeiss). Acquisition was performed with a Quemesa CCD
260 camera and the iTEM software (Emsis).
261
262 **TUNEL assay**
263 Kidneys were fixed in 10% (v/v) Neutral-buffered Formalin overnight, dehydrated and
264 embedded in paraffin. 5-µm sections were rehydrated, stained using the ApopTag Plus
265 Peroxidase In Situ Apoptosis Detection Kit (Merck Millipore) according to the manufacturer's
266 instructions and counterstained with haematoxylin (Fluka) for 2 min. Images were taken with
267 an Axio Scope.A1 microscope using the Zen software (Zeiss).
268
269 **Immunoblotting**
270 Whole kidneys were homogenized and protein was extracted from 20 mg of tissue in 1 ml RIPA
271 buffer supplemented with protease inhibitors (Roche) for 2 hrs. 10 µg of protein was separated
272 by SDS-PAGE using a 10% separating and a 4.5% stacking gel and transferred to a PVDF
273 membrane with 0.2 µm pore size (Roth) via a semidry transfer. The membrane was blocked
274 with 5% skim milk in TBS-T, cut in half and probed with the mouse anti-β-catenin (1:1000, BD
275 Transduction Laboratories, 610153) or mouse anti-α-Tubulin (1:10000, Sigma-Aldrich, T9026)
276 antibody overnight and with the peroxidase-conjugated donkey anti-mouse antibody (1:5000,
277 Jackson) for 1 hr. The antibodies were diluted in 5% BSA in TBS-T. Bands were visualized
278 using the Western Lightning Plus-ECL substrate (PerkinElmer) for 5 min and a Fusion SL
279 imaging system (Vilber).
280
281 **Real-time qPCR**
282 Total RNA from the organoids and whole mouse kidneys was isolated using TRIzol
283 (Invitrogen), and 1 µg/20 µl of RNA was reversely transcribed to cDNA using MMLV reverse
284 transcriptase (Promega) according to the manufacturer's instructions. Real-time qPCR
285 reactions were performed in a CFX96-C1000 thermal cycler (Bio-Rad) with the PowerUp

286 SYBR Green Master Mix (Applied Biosystems) and 10 μM exon-exon junction-spanning
287 primers, using a standard protocol with 44 cycles according to the manufacturer's instructions.
288 Primer sequences are listed in the Table 2. Primer specificity was tested by melting curve
289 analyses and running reactions with a negative control (without cDNA). Relative mRNA
290 expression values were normalized to the endogenous control Gapdh using the 2-ΔΔCt
291 method.
292
293 **Table 2**. **Primer sequences for real-time qPCR.**

Gene	Forward primer 5'-3'	Reverse primer 5'-3'
Krt8	CTCAAAGGCCAGAGGGCATC	TTAATGGCCATCTCCCCACG
Krt18	ACTGGTCTCAGCAGATTGAGG	CCGAGGCTGTTCTCCAAGTT
Cldn4	CTTCATCGGCAGCAACATCG	GATGACCATAAGGGCTCGGG
Abcb1b	AGTGGCTCTTGAAGCCGTAA	AAACTCCATCACCACCTCACG
Slc3a1	AAAATGCCTTGACTGGTGGCA	CCTCAACAGCGTATCTGAAGTCT
Slc40a1	GAGCCAGTGTCCCCAACTAC	CTTGCAGCAACTGTGTCACC
Aqp3	ATCGTTGTGGGGAGATGCTT	ACCAAGATGCCAAGGGTGAC
Atp6ap2	GGCAAAACAAGAGAACACCCA	CCAAGGCCAAGCCGATCATA
Wnk1	CCTCAAGTATGGCACAGGGG	GCTGTATTCCCTGCTGCTGA
Dkk1	CGGGGGATGGATATCCCAGA	ACGGAGCCTTCTTGTCCTTTG
Axin2	GCGCTTTGATAAGGTCCTGG	TCATGTGAGCCTCCTCTCTTTT

Cyclin D1	CTGGATGCTGGAGGTCTGTGA	AGGGGGTCCTTGTTTAGCCAG
Myc	TTGGAAACCCCGCAGACAG	GCTGTACGGAGTCGTAGTCG
Hey1	GAGCGTGAGTGGGATCAGTG	GCTTAGCAGATCCCTGCTTCT
Hes1	CTGGTGCTGATAACAGCGGA	GGAATGCCGGGAGCTATCTT
Hey3 (Heyl)	GTCTTGCAGATGACCGTGGA	CGGGCATCAAAGAACCCTGT
Ca9	GTCATTGGAGCTATGGAGG	CTCATAACCCAGAAGTTCCAG
Hk2	GTGACAGACAATGGTCTCCAGAG	GCCAGGCATTCGGCAATG
Pdk1	GCAGTTCCTGGACTTCG	CAATCTAACAGGCAACTCTTG
Ldha	GATGGATCTCCAGCATGGCAG	GTGATAATGACCAGCTTGGAGTTCG
Glut1	GCTATAACACTGGTGTCATCAACG	CGTGGTGAGTGTGGTGGATG
Vegfa	CAGGCTGCTGTAACGATGAA	TTTCTTGCGCTTTCGTTTTT
Ngal	ACAACCAGTTCGCCATGGTA	AAGCGGGTGAAACGTTCCTT
Kim-1	CAGGGTCTCCTTCACAGCAG	CCACCACCCCCTTTACTTCC
Gsta1	AGCCCGTGCTTCACTACTTC	CAATCTCCACCATGGGCACT
Il1b	TTCAGGCAGGCAGTATCA	CCAGCAGGTTATCATCATCA
Cd11b	CCACACTAGCATCAAGGGCA	GCTTCACACTGCCACCGT

Ly6c	GCAGTGCTACGAGTGCTATGG	ACTGACGGGTCTTTAGTTTCCTT
Icam1 (Cd54)	GTCCGCTGTGCTTTGAGAAC	GAGGTCCTTGCCTACTTGCT
Cd68	ACTTCGGGCCATGTTTCTCT	GCTGGTAGGTTGATTGTCGT
Ccr2 (Cd192)	GCCATCATAAAGGAGCCATACC	ATGCCGTGGATGAACTGAGG
Vim	TGGATCAGCTCACCAACGAC	AAGGTCAAGACGTGCCAGAG
Fn1	ATGAGAAGCCTGGATCCCCT	GGAAGGGTAACCAGTTGGGG
a-sma	ACATCAAGGAGAAGCTGTGCT	TTTCGTGGATGCCCGCTG
Col1a1	CATGAGCCGAAGCTAACCCC	GGGTTTCCACGTCTCACCAT
Col3a1	AGTGGGCATCCAGGTCCTAT	GGGTGAAAAGCCACCAGACT

Genomic DNA PCR

Genomic DNA was isolated from whole kidneys using the GeneJET Genomic DNA Purification Kit (Thermo Fisher Scientific) according to the manufacturer's instructions. β-catenin and Vhl alleles were amplified using 100 ng of DNA, 10 µM primers and a standard protocol with 50 and 40 cycles and annealing temperature of 65°C and 56°C, respectively. A forward primer 5'-3': GGTACCTGAAGCTCAGCG-CACAGCTG and a reverse primer 5'-3': ACGTGTGGCAAGTTCCGCGTCATCC were used to amplify the β-catenin allele (23). A forward primer 1 5'-3': CTGGTACCCAC-GAAACTGTC, a forward primer 2 5'-3': CTAGGCACCGAGCTTAGAGGTTTGCG and a reverse primer 5'-3': CTGACTTCCACTGATGCTTGTCACAG were used to amplify the Vhl allele (37).

Drug response assay

307 Single cells were seeded at 15,000 cells per well in 9 µl Matrigel (75%, Corning) lenses in 96-
308 well plates and overlayed with 100 µl organoid medium. After 24 hrs, medium was replaced
309 with fresh medium containing ICG-001 (Biochempartner) or LF3 (Selleckchem). Medium was
310 changed every other day. CellTiterGlo assay (Promega) was performed after 6 days according
311 to the manufacturer's instructions.
312
313 **Blood assays**
314 Blood was collected from hearts of freshly sacrificed mice to tubes coated with 0.5 M EDTA
315 pH 8 (Invitrogen) to prevent clotting. BUN concentrations were measured using the i-STAT 1
316 System with the CHEM8+ cartridges for patient testing (Abbott) according to the
317 manufacturer's instructions. For plasma collection, cells and platelets were pelleted from the
318 blood by centrifugation for 15 min at 2000 g. EPO concentrations in supernatants (plasma)
319 were measured using the Quantikine Mouse Erythro-poietin Immunoassay (R&D Systems)
320 according to the manufacturer's instructions.
321
322 **Descriptive statistics and significance testing**
323 The Pearson correlation matrix (coefficient) was calculated by the cor function of the base R
324 package between all samples of mouse kidney epithelia (control kidney, CK), early passage
325 organoids (OEP) and long-term passage organoids (OLP) based on normalized log2 intensity
326 values for 9,000 proteins and 16,000 phosphorylation sites detected in the mass spectrometry
327 analysis. The matrix was plotted using the pheatmap R package. For the functional annotation
328 clustering of the most upregulated proteins using DAVID bioinformatic tool (DAVID
329 Bioinformatics Resources 6.8, NIAID/NIH), 9,000 proteins detected in the proteomic analysis
330 were subjected to both the 0.1% FDR cutoff (adjusted P-value < 0.001) and log2 fold change
331 cutoff of > 0.5 for both OEP over CK and OLP over CK. 722 proteins were selected. Using the
332 entire mouse (Mus musculus) proteome as a background for the UNIPROT_ACCESSION
333 identifier, 671 proteins (DAVID IDs) were identified and analyzed. Defined DAVID defaults
334 were used and the Enrichment Thresholds (EASE Scores, modified Fisher-exact P-values)

335 and adjusted P-values (Benjamini-Hochberg correction) for all terms in each cluster were
336 subjected to the cutoff of < 0.001. 10 clusters were determined. The overall enrichment score
337 for each cluster was calculated based on the Enrichment Thresholds for all terms. The most
338 enriched term was selected to represent each cluster based on the lowest adjusted P-value.
339 All other statistical analyses were performed in GraphPad Prism (GraphPad). All data are
340 presented as mean ± SD (error bars), unless otherwise stated. To assess the normal
341 distribution of the data, the Shapiro-Wilk test ($\alpha = 0.05$) was performed. The unpaired, two-
342 tailed Student's t-test and the ordinary one-way ANOVA followed by the Dunnett's multiple
343 comparison were used to analyze data, which passed the normality test. To compare groups,
344 which did not pass the normality test, the alternative non-parametric Kruskal-Wallis test
345 followed by the Dunn's multiple comparison were performed. The ordinary one-way ANOVA
346 fol-lowed by the Dunnett's multiple comparison were used to analyze the real-time qPCR data
347 on the organoids. A P-value < 0.05 was considered statistically significant. IC50 values were
348 calculated by a non-linear regression analysis of the response and log10 of the inhibitor
349 concentration fitting a curve with a variable slope (four parameters). Statistical details of the
350 experiments can be found in the figure legends.
351

352 # Results

353 **Self-renewal of long-term organoid cultures from adult mouse kidneys**

354 We isolated single epithelial cells from whole adult mouse kidneys and established 3D
355 organoid cultures with high efficiency in Matrigel and serum-free conditions (n = 20). The
356 protocol was adapted to specific needs of kidney stem/progenitor cells (Table 1). Within 14
357 days of culture, single cells grew continuously and formed organoids with sizes up to 1.5 mm
358 in diameter (Fig 1A). By H&E staining, we classified three organoid types: cystic organoids
359 with one or more cell layers and a single lumen (with few organoids containing one or two
360 additional smaller lumina), solid filled organoids, and alveolar organoids with multiple lumina,
361 accounting for 65%, 25% and 10% (Fig 1B).

362

363 Organoid formation from single cells was five times higher in the first passage in comparison
364 to freshly seeded cultures (Fig 1C and D), indicating self-renewal capacity of cells. For
365 maintenance, the organoids were serially passaged starting from small cell clusters (Fig 1E),
366 which allowed to culture them for at least 3.5 months (passage 12, S1A Fig). Organoid cultures
367 were established from mice with a mixed C57BL/6J and FVB/NJ background, but they could
368 also be generated from C57BL/6J mice with similar efficiency (S1B Fig). Hence, we created
369 self-renewing long-term organoids from single adult mouse kidney epithelial cells, which
370 predominantly exhibited cystic morphologies, consistent with organoid cultures derived from
371 other adult organs (8).

372

373 **Fig 1.** Self-renewal of organoid cultures from adult mouse kidneys. (A) Brightfield images acquired on consecutive
374 days of an organoid formed from a single freshly seeded cell. (B) H&E staining showing freshly seeded organoids
375 with cystic (left), solid (middle) and alveolar (right) morphology. (C) Brightfield images of a freshly seeded (left) and
376 a once passaged (right) organoid culture grown from 10^5 single cells. (D) Quantification of organoid numbers in a
377 freshly seeded and passage 1 culture. (E) Brightfield image of a serially passaged organoid culture after 5
378 passages. Data information: scale bars, 100 µm in A, 50 µm in B, 500 µm in C and E. 20 freshly seeded organoid
379 cultures were established in total. In A, one independent replicate was examined. For quantification in B, 180
380 organoids were counted in total. One independent replicate was examined. For quantification in C and D, 10^5 cells

were seeded and the organoids with diameters ≥ 100 µm were counted after 14 (freshly seeded cells) or 7 (passaged cells) days of culture (6 wells, technical replicates). One independent replicate was examined. In D, the graph shows mean ± SD (error bars). Data passed the Shapiro-Wilk normality test (α = 0.05). The unpaired, two-tailed Student's t-test was performed; P-value, < 0.0001, ****p < 0.0001. In E, three independent replicates were examined.

Examination of kidney organoids by deep proteomic and phosphoproteomic analyses revealed that the cultures closely resembled adult mouse kidney epithelia and were phenotypically stable over time

We performed mass spectrometry-based deep bulk proteomics and phosphoproteomics. Three independent replicates of adult kidney epithelial cells (control kidney), early passage organoids (passage 2, 1-month culture) and long-term passage organoids (passage 12, 3.5-month culture) were compared. To prepare control samples, Epcam-positive kidney epithelial cells were MAC-sorted from freshly isolated single cell suspensions from whole mouse kidneys, similar to a protocol for preparing adult human kidney organoids (10). We could detect 9,000 proteins and 16,000 phosphorylation sites of these proteins, which is the maximum coverage currently possible (32). We calculated Pearson correlations between the samples and found high correlations, at least 0.8, between adult kidney epithelial cells (control kidney, CK) and both early passage organoids (OEP) and long-term passage organoids (OLP) for both proteome (Fig 2A) and phosphoproteome (Fig 2B). This indicated that the organoids closely resembled kidney epithelia. Moreover, OLP recapitulated OEP for both proteome (Fig 2A) and phosphoproteome (Fig 2B), as shown by correlations of around 1, confirming that organoid cultures were phenotypically stable over time.

Kidney organoids displayed enhanced proliferation, and upregulation of stem cell-associated Wnt, Notch and Yap signaling

We also recorded the importance of many upregulated proteins in the organoids in comparison to kidney epithelia. Using a bioinformatic tool for functional annotation clustering, DAVID, we discovered 10 biological processes in the organoids, which were governed by upregulated

410 proteins (Fig 2C). The top three enriched processes were cell cycle, ribosomal activity and
411 DNA replication, which indicated the presence of proliferating cells. We confirmed this by BrdU
412 incorporation in nuclei (marked in magenta, Fig 2D). In line with the self-renewal capacity,
413 enhanced proliferation suggested enrichment in stem/progenitor cells in the organoids and
414 thus the recapitulation of the potential of the adult kidney for renewal. DAVID analysis also
415 revealed enrichment in cell polarity-related proteins of adherens junctions and basement
416 membranes (Fig 2C).
417
418 By manual curation, proteomic analysis in both OEP and OLP revealed upregulation of
419 components of stem cell-associated Wnt (Fig 2E) and Notch (Fig 2F) signaling. Upregulated
420 Wnt components included ligands Wnt4, Wnt7b and Wnt10a, co-receptors Lrp5 and Lrp6, the
421 destruction complex disassembly-mediating protein Dvl2 and targets Axin2, Birc5, Cd44 and
422 Cyclin D1 (Ccnd1). Upregulated Notch components included the ligand Jag2, receptors
423 Notch1, Notch2 and Notch3, the S2 cleavage-mediating metalloproteinase Adam17, S3
424 cleavage γ-secretase complex-related Aph1a and Ncstn as well as co-activators Rbpj, Maml1,
425 Maml2 and Kat2b. Proteomic analysis also revealed in both OEP and OLP upregulation of
426 another stem cell-associated signaling system, Yap (S2 Fig). Upregulated Yap components
427 were direct Yap targets. Thus, the organoids and adult mouse kidney epithelia largely shared
428 proteome and phosphoproteome patterns, which remained unchanged over passages.
429 Moreover, strong proliferation of the organoids and upregulation of the Wnt, Notch and Yap
430 signaling systems were the signs of the enrichment in stem/progenitor cells.
431
432 **Fig 2. Kidney organoids closely resemble adult mouse kidney epithelia, are phenotypically stable over time,**
433 **and display enhanced proliferation and stem cell-associated Wnt and Notch signaling.** (A) Heatmap for the
434 Pearson correlation matrix (coefficient) of the expression levels of 9,000 proteins between all samples of mouse
435 kidney epithelia (control kidney, CK), early passage organoids (OEP) and long-term passage organoids (OLP). The
436 experimental columns were correlated against each other. (B) Heatmap for the Pearson correlation matrix
437 (coefficient) of the phosphorylation levels of 16,000 corresponding phosphorylation sites between all samples of
438 mouse kidney epithelia (control kidney, CK), early passage organoids (OEP) and long-term passage organoids

439 (OLP). The experimental columns were correlated against each other. (C) Functional annotation clustering of the
440 most upregulated proteins in the organoids using DAVID bi-oinformatic tool. Shown are 10 most enriched clusters,
441 based on the overall enrichment scores, with their representative terms (biological processes), based on the
442 adjusted P-values. (D) 2D immunofluorescence for BrdU (magenta) of an organoid culture. (E) Proteomic heatmap
443 for components of Wnt signaling in both early (OEP) and long-term (OLP) passage organoids in comparison to
444 mouse kidney epithelia (control kidney, CK). (F) Proteomic heatmap for components of Notch signaling in both early
445 (OEP) and long-term (OLP) passage organoids in comparison to mouse kidney epithelia (control kidney, CK). Data
446 information: scale bars in D, 50 μm. Nuclei are counterstained with DAPI. Three independent replicates were
447 examined. In E and F, the heatmaps show normalized log2 intensity values for three independent replicates of CK,
448 OEP and OLP. A 5% FDR (adjusted P-value < 0.05) cutoff and a log2 fold change cutoff of > 0 were applied for
449 both OEP over CK and OLP over CK. The values were scaled (z-score by row) with breaks from ≤ -2 to ≥ 2.
450

451 **Kidney organoids contained differentiated and polarized tubular epithelial cells**

452 Ubiquitous staining of Pax8 in nuclei (marked in brown) confirmed that organoid cells were of
453 kidney origin (Fig 3A). The organoids contained differentiated kidney epithelial cells, as
454 indicated by the presence of adherens junctions between lateral membranes of neighboring
455 cells, which were positive for E-cadherin (E-cad, marked in orange, Fig 3B), and by
456 upregulation of Keratin 8 (Krt8), Claudin 4 (Cldn4) and *Keratin 18 (Krt18)* (Fig 3C). In line with
457 DAVID analysis, cells displayed pronounced epithelial polarity, as shown by the location of
458 Laminin in the basal laminae (marked in green) and of Zo-1-positive tight junctions at the apical
459 sides (marked in red) (Fig 3D).
460

461 Cells were positive either for Lotus Tetragonolobus Lectin (LTL, marked in red), a marker of
462 proximal tubular epithelial cells, or Peanut Agglutinin (PNA, marked in green), a marker of
463 epithelial cells of distal nephrons, i.e. distal tubules and collecting ducts, and both markers
464 were detected within the same organoids (Fig 3E). Proteomic analysis revealed enrichment in
465 48 membrane transporters in both OEP and OLP (Fig 3F), including known transporters of
466 proximal tubular cells such as amino acid transporters Slc1a4 and Slc1a5, the glucose
467 transporter Slc2a1, the myo-inositol transporter Slc5a11, ion transporters Slc12a6 and
468 Slc26a2, zinc transporters Slc30a6 and Slc39a10 and efflux transporters Abcb1b, Abcc3 and

469 Abcc4. In addition, known transporters of distal nephrons were upregulated, including Slc6a9,
470 a glycine transporter of distal and connecting tubules, and ion transporters of collecting ducts,
471 Slc4a1ap, Slc4a7, Atp6ap2 and Trpv4. Proton transporters Atp6v0a1 and Atp6v0a2, which are
472 present in both proximal tubules and collecting ducts, were also enriched. Proteomic analysis
473 also revealed upregulation of Wnk1, a common cytoplasmic marker (a kinase) of distal and
474 connecting tubules and of cortical collecting ducts, and Gata3, a nuclear marker (a transcription
475 factor) of collecting ducts (Fig 3G). In LTL/PNA-double-positive organoids, we confirmed in a
476 subset of LTL-positive cells expression of Abcb1b (marked in cyan), another marker of
477 proximal tubular cells, which did not overlap with PNA-positive cells of distal nephrons (Fig
478 3H). In these organoids, we also detected in a subset of PNA-positive cells expression of
479 Aquaporin 3 (Aqp3, marked in magenta), a marker of principal cells of collecting ducts, which
480 was mutually exclusive with LTL-positive cells (Fig 3I). We also observed mutually exclusive
481 expression of LTL and PNA in solid and alveolar organoids (S3A Fig). Whole-mount confocal
482 microscopy confirmed expression of LTL, PNA and E-cad in 3D reconstructed cystic organoids
483 (S3B Fig and C, and S1 Video).
484
485 **Fig 3. Kidney organoids exhibit markers of differentiated and polarized tubular epithelial cells.** (A)
486 Immunohistochemistry for Pax8 (brown) of an organoid culture. (B) 2D immunofluorescence for E-cad (orange) of
487 an organoid culture. (C) Proteomic heatmaps for Krt8 and Cldn4 in both early (OEP) and long-term (OLP) passage
488 organoids in comparison to mouse kidney epithelia (control kidney, CK; upper part), and real-time qPCR analysis
489 of gene expression of Krt18 in both early (OEP) and long-term (OLP) passage organoids in comparison to whole
490 mouse kidney cells (control kidney, CK; lower part). (D) 2D immunofluorescence for Laminin (green) and Zo-1 (red)
491 of an organoid culture. (E) 2D immunofluorescence for LTL (red) and PNA (green) of an organoid culture. (F)
492 Proteomic heatmap for 48 membrane transporters in both early (OEP) and long-term (OLP) passage organoids in
493 comparison to mouse kidney epithelia (control kidney, CK). (G) Proteomic heatmaps for Wnk1 and Gata3 in both
494 early (OEP) and long-term (OLP) passage organoids in comparison to mouse kidney epithelia (control kidney, CK).
495 (H) 2D immunofluorescence for Abcb1b (cyan), LTL (red) and PNA (green) of an organoid culture. (I) 2D
496 immunofluorescence for Aqp3 (magenta), LTL (red) and PNA (green) of an organoid culture. Data information: scale
497 bars in A/B/D/E/H/I, 50 μm. In A, nuclei are counterstained with haematoxylin; in B/D/E/H/I, nuclei are
498 counterstained with DAPI. In C, the graph shows mean ± SD (error bars). The ordinary one-way ANOVA followed

499 by the Dunnett's multiple comparison to CK were performed; both P-values, 0.0001, ****p < 0.0001. In C/F/G, the
500 heatmaps show normalized log2 intensity values for three independent replicates of CK, OEP and OLP. A 5% FDR
501 (adjusted P-value < 0.05) cutoff and a log2 fold change cutoff of > 0 were applied for both OEP over CK and OLP
502 over CK. Values were scaled (z-score by row) with breaks from ≤ -2 to ≥ 2. In A/B/D/E/H/I, three independent
503 replicates were examined. For the real-time qPCR analysis of Krt18 in C, three independent replicates in technical
504 triplicates were examined.
505
506 Transmission electron microscopy confirmed epithelial cell polarity and complexity of the
507 organoids. Cystic organoids developed microvilli (MV) at apical membranes towards the lumen
508 (L), a typical feature of proximal tubular cells (S4A Fig). At the basal side, microvilli-free basal
509 laminae (arrowhead) and filopodia (F) were seen (S4A Fig). Junctional complexes (JC)
510 between neighboring cells, which are involved in barrier formation, were present at lateral
511 membranes at the luminal side. JC included from the apical to basal side: tight junctions
512 (zonula occludens, black asterisk), adherens junctions (belt desmosomes, zonula adhaerens,
513 white asterisk), spot desmosomes (macula adhaerens, red asterisks) and closely aligned or
514 nearly fused lateral membranes (white and black arrowheads, respectively) (S4B Fig). At the
515 basal side, we observed spot desmosomes (red asterisk) and closely aligned or nearly fused
516 lateral membranes (white and black arrowheads, respectively) (S4C Fig). Endocytic events,
517 i.e. clathrin-coated pits with diameters of 100 nm, which are typical for proximal tubular cells
518 (38), were observed at apical and lateral membranes (marked by arrowheads, S4D Fig).
519 Together, apart from stem/progenitor cells, kidney organoids contained differentiated tubular
520 epithelial cells with apical and basal polarity and complex intercellular junctions.
521
522 **Wnt signaling controlled self-renewal, growth and differentiation of kidney organoids**
523 We examined the dependence of the organoids on Wnt signaling by removing or adding single
524 Wnt activators and by blocking Wnt with small-molecule inhibitors. Withdrawal of the Wnt
525 activator R-spondin-1 reduced organoid numbers (self-renewal) and sizes. Addition of the Wnt
526 ligand Wnt3a did not improve organoid yield (Fig 4A and B), possibly due to autocrine supply
527 of Wnt4, Wnt7b or Wnt10a. Treatments with ICG-001, an inhibitor that blocks β-catenin-Tcf-

528 mediated transcription, and with LF3, another β-catenin-Tcf inhibitor developed in our
529 laboratory (39) (Fig 4C), produced concentration-dependent inhibition of organoid growth (Fig
530 4D and F) and concentration-dependent decrease in cell viability (Fig 4E and G). By H&E
531 staining, we observed upon R-spondin-1 removal a switch from predominant cystic to fully solid
532 organoids, while treatment with ICG-001 at IC50 did not result in morphological changes (Fig
533 4H). Transition to solid morphologies induced by R-spondin-1 withdrawal prompted to study
534 the importance of Wnt signaling for the control of organoid differentiation. By real-time qPCR,
535 we examined in the organoids upon R-spondin-1 removal or ICG-001 treatment expression of
536 selected genes, which are induced in differentiated kidney tubular epithelial cells. We found
537 increases in abundance of *Krt8*, *Krt18* and *Cldn4* (Fig 4I). We also observed upregulation of
538 proximal tubule genes *Abcb1b*, *Slc3a1* and *Slc40a1* (Fig 4J) as well as of distal nephron genes
539 *Aqp3*, *Atp6ap2* and *Wnk1* (Fig 4K). Immunofluorescence staining confirmed upregulation of
540 Aqp3 in these organoids (Fig 4L). Altogether, mouse kidney organoid cultures required Wnt
541 signaling to promote self-renewal, growth and differentiation into proximal and distal nephron
542 lineages.
543
544 **Fig 4. Wnt signaling controls kidney organoid formation, growth and differentiation.** (A) Organoid numbers
545 per well with indicated growth factor combinations (withdrawal or addition). (B) Diameters (μm) of the organoids
546 (single dots) from wells with indicated growth factor combinations (withdrawal or addition). (C) Scheme of Wnt
547 signaling with a common target for the small-molecule inhibitors ICG-001 and LF3. (D and F) Brightfield images of
548 organoid cultures at indicated ICG-001 (D) and LF3 (F) concentrations (μM) on day 6 of treatment. (E and G) Curves
549 showing the dependence of organoid viability (fold change ATP luminescence) on log10 ICG-001 (E) and LF3 (G)
550 concentration (μM) on day 6 of treatment. (H) H&E staining of organoid cultures upon R-spondin-1 removal or
551 treatment with ICG-001 at IC50. (I) Real-time qPCR analysis of gene expression of differentiation markers Krt8,
552 Krt18 and Cldn4 in the organoids upon R-spondin-1 removal or treatment with ICG-001 at IC50. (J) Real-time qPCR
553 analysis of gene expression of markers of proximal tubular cells, Abcb1b, Slc3a1 and Slc40a1, in the organoids
554 upon R-spondin-1 removal or treatment with ICG-001 at IC50. (K) Real-time qPCR analysis of gene expression of
555 markers of distal nephrons, Aqp3, Atp6ap2 and Wnk1, in the organoids upon R-spondin-1 removal or treatment
556 with ICG-001 at IC50. (L) 2D immunofluorescence for Aqp3 (magenta) in the organoids upon R-spondin-1 removal
557 or treatment with ICG-001 at IC50. Data information: in A and B, culture medium containing DMEM/F12 with

558 GlutaMax, HEPES, N-acetylcysteine, B27, N2, nicotinamide, hydrocortisone (HC) and prostaglandin E2 (PGE2) is
559 common to all the conditions. For quantification, 10^5 cells were freshly seeded and the organoids with diameters ≥
560 200 μm were counted after 14 days of culture. The graphs show mean ± SD (error bars). In A, data passed the
561 Shapiro-Wilk normality test (α = 0.05). The ordinary one-way ANOVA followed by the Dunnett's multiple comparison
562 to complete organoid medium (Ctrl, first from the left) were performed; P-values from left to right, 0.0001, 0.2132;
563 ****p < 0.0001, ns: non-significant. In B, data did not pass the Shapiro-Wilk normality test (α = 0.05). The alternative
564 non-parametric Kruskal-Wallis test followed by the Dunn's multiple comparison to complete organoid medium (Ctrl,
565 first from the left) were performed; P-values from left to right, 0.0090, 0.0129; **p < 0.01, *p < 0.05. In A and B, three
566 independent replicates with 6 technical replicates (wells) were examined and collectively shown. Ctrl in D-G, the
567 organoids cultured in complete medium and treated with DMSO at re-spective concentrations. Scale bars in D and
568 F, 500 μm. In E and G, the curves show mean ± SD (error bars). In E, ICG-001 produced the IC50 of 14.66 μM; in
569 G, LF3 produced the IC50 of 15.72 μM. In D-G, three independent replicates in technical triplicates (wells) were
570 examined. Ctrl in H-L, the organoids cultured in complete medium and treated or not with DMSO at a respective
571 concentration. Scale bars in H, 100 μm. Three independent replicates were examined. In I-K, the graphs show
572 mean ± SD (error bars). The ordinary one-way ANOVA followed by the Dunnett's multiple comparison to Ctrl were
573 performed; P-values from left to right in I; 0.0004, 0.0001 for Krt8; 0.0153, 0.0002 for Krt18; 0.0002, 0.0003 for
574 Cldn4; in J: 0.0001, 0.0001 for Abcb1b; 0.0005, 0.0164 for Slc3a1; 0.0910, 0.0001 for Slc40a1; in K: 0.0001, 0.0001
575 for Aqp3; 0.0014, 0.0001 for Atp6ap2; 0.001, 0.0001 for Wnk1; ****p < 0.0001, ***p < 0.001, **p < 0.01, *p < 0.05,
576 ns: non-significant. Three independent replicates in technical triplicates were examined. Scale bars in L, 50 μm.
577 Three independent replicates were examined.
578

579 **Generation of double kidney mutants in mice to model stem cell-driven development of**
580 **human ccRCC**

581 To investigate a relation between Wnt-high and Notch-high kidney stem/progenitor cells
582 enriched in our mouse kidney organoids and in human ccRCC, we genetically modified Wnt
583 and Notch signaling in mice. We generated two types of double mouse mutants by the loxP-
584 mediated recombination of adult kidney epithelial cells: i) Wnt-β-catenin gain of function
585 combined with Notch1 intracellular domain (N1icd) gain of function, hereafter called β-catenin-
586 GOF; Notch-GOF, and ii) Von Hip-pel-Lindau loss of function combined with Wnt-β-catenin
587 gain of function, hereafter called Vhl-LOF; β-catenin-GOF. For the details of the generation of

588 the genetic system and mutants, see Fig 5A. Vhl-LOF; Notch-GOF mutant mice had already
589 been established using different Cre systems (19,20).
590
591 To examine cellular patterns of recombination, we established Pax8-rtTA(+); LC1-Cre(+);
592 LacZ(+) reporter mice, which carried a loxP-flanked stop cassette upstream of the LacZ
593 sequence encoding β-galactosidase. After doxycycline treatment of one-month-old mice,
594 immunohistochemistry revealed Cre expressed in nuclei of kidney epithelial cells in both
595 cortical and medullary parts, including proximal tubular cells (Fig 5B). The Cre pattern was
596 confirmed by cytoplasmic LacZ staining after treatment with X-gal. Glomeruli (marked by black
597 lines) remained negative for Cre and LacZ. We did not observe Cre- and LacZ-positive cells in
598 doxycycline-treated Pax8-rtTA(-); LC1-Cre(+); LacZ(+) control kidneys, indicating that the
599 genetic system was not leaky. Then, we treated with doxycycline critical one-month-old Pax8-
600 rtTA(+); LC1-Cre(+); β-catenin loxP/wt; Notch loxP/wt (β-catenin-GOF; Notch-GOF) mice and
601 Pax8-rtTA(+); LC1-Cre(+); Vhl loxP/loxP; β-catenin loxP/wt (Vhl-LOF; β-catenin-GOF) mice (n
602 = 20 per line). We also treated controls carrying β-catenin- and Notch- or Vhl- and β-catenin-
603 loxP alleles, but no Pax8-rtTA or LC1-Cre (n = 20).
604
605 We examined in kidney mutants the recombination of β-catenin, Notch and Vhl alleles on
606 genomic DNA, protein and mRNA target gene levels. We detected DNA bands of recombined
607 (700 bp) and wild-type (900 bp) β-catenin alleles in both mutants, as compared to control
608 kidneys with only wt alleles (Fig 5C). In Vhl-LOF; β-catenin-GOF mutant, we detected DNA
609 bands of recombined (260 bp) and non-recombined loxP (460 bp) Vhl alleles, as opposed to
610 control kidneys with only loxP alleles (Fig 5D). Recombined β-catenin protein accumulated in
611 both mutants (72 kDa band), as compared to controls with only wt protein (95 kDa band) (Fig
612 5E). We observed nuclear N1icd in β-catenin-GOF; Notch-GOF mutant, but not in controls (Fig
613 5F). We found upregulation of β-catenin target genes *Dkk1*, *Axin2*, *Cyclin D1* and *Myc* in β-
614 catenin-GOF; Notch-GOF (Fig 5G) and Vhl-LOF; β-catenin-GOF (Fig-ure 5H) mutants, as
615 opposed to controls. Expression of Notch target genes *Hey1*, *Hes1* and *Hey3* in β-catenin-

616 GOF; Notch-GOF mutant (Fig 5I) and of Hif-1α/2α target genes *Ca9*, *Hk2*, *Pdk1*, *Myc*, *Ldha*,
617 *Cyclin D1*, *Glut1* and *Vegfa* in Vhl-LOF; β-catenin-GOF mutant (Fig 5J) also increased, as
618 compared to controls. Thus, our data show that in mice targeted mutagenesis in adult kidney
619 epithelial cells occurred and that mutant cells were not cleared over time.

620

621 **Fig 5. Generation of double kidney mutants in mice.** (A) Scheme of the genetic system to generate mutant
622 kidneys. (B) Time course and pattern of recombination in kidneys of Pax8-rtTA(+); LC1-Cre(+); LacZ(+) reporter
623 mice. (C) PCR for DNA recombination of the loxP-flanked exon 3 sequence of β-catenin gene in β-catenin-GOF;
624 Notch-GOF and Vhl-LOF; β-catenin-GOF mutant kidneys (700 bp) versus controls (900 bp). (D) PCR for DNA
625 recombination of the loxP-flanked promoter-exon 1 sequence of Vhl gene in Vhl-LOF; β-catenin-GOF mutant
626 kidneys (260 bp) versus controls (460 bp). (E) Immunoblotting for recombination of β-catenin in β-catenin-GOF;
627 Notch-GOF and Vhl-LOF; β-catenin-GOF mutant kidneys (72 kDa) versus controls (95 kDa). (F)
628 Immunohistochemistry for nuclear N1icd in β-catenin-GOF; Notch-GOF mutant cortical kidneys versus controls. (G)
629 Fold change of expression of selected β-catenin target genes in β-catenin-GOF; Notch-GOF mutant kidneys versus
630 controls. (H) Fold change of expression of selected β-catenin target genes in Vhl-LOF; β-catenin-GOF mutant
631 kidneys versus controls. (I) Fold change of expression of selected Notch target genes in β-catenin-GOF; Notch-
632 GOF mutant kidneys versus controls. (J) Fold change of expression of selected Hif-1α/2α target genes in Vhl-LOF;
633 β-catenin-GOF mutant kidneys versus controls. Data information: abbreviation in A; dox, doxycycline. Scale bars in
634 B, 100 μm. In the upper panel, nuclei are counterstained with haematoxylin; in the lower panel, nuclei are
635 counterstained with nuclear fast red. Glomeruli are marked by black lines. Two independent replicates of Pax8-
636 rtTA(+); LC1-Cre(+); LacZ(+) mice and one of Pax8-rtTA(-); LC1-Cre(+); LacZ(+) controls were examined.
637 Abbreviations in C-E; wt, wild-type; ex3 del, exon 3 deletion; prom-ex1 loxP/del, promoter-exon 1 loxP/deletion.
638 Scale bars in F, 100 μm. Nuclei are counterstained with haematoxylin. In C-F, three independent replicates per line
639 were examined. In G-J, graphs show mean + SD (error bars). Three independent replicates (mice, dots) in technical
640 triplicates were analyzed. No statistical test was performed because of high inter-mouse variance. However,
641 increase trends were observed.

642

643 **No tumorigenesis was observed in double mutant kidneys**

644 Mutant mice were examined 1-8 months after the doxycycline pulse and exhibited severe
645 illness symptoms. These included reduced body weight (Fig 6A) and enlarged spleens, called
646 splenomegaly (Fig 6B and D). Mutant kidneys appeared to be of smaller sizes (Fig 6B), but

647 their relative weight did not change (Fig 6C). Kidneys and spleens of mutant mice were pale,
648 suggesting anemia (Fig 6B).
649
650 We performed Periodic acid-Schiff (PAS) staining of mutant kidneys, which detects tissues
651 with high proportions of sugar macromolecules such as tubular and glomerular basement
652 membranes and brush borders of proximal tubules. Examination by pathologists did not reveal
653 tumors or premalignant lesions such as dysplasia or adenomas, even after 8 months after the
654 doxycycline pulse. Non-neoplastic pathological changes of kidney tissues like cysts,
655 hypertrophy, necrosis, dilation or atrophy of tubules as well as tubule-interstitial fibrosis were
656 neither present (Fig 6E). Nuclear crowding was observed in some tubules in the cortex in β-
657 catenin-GOF; Notch-GOF, but not in Vhl-LOF; β-catenin-GOF kidneys (Fig 6F). We conducted
658 Ki67 staining for proliferating cells at the G1, S, G2 and M phases of the cell cycle. None of
659 mutant kidneys, even after 8 months after the doxycycline pulse, exhibited higher numbers of
660 Ki67-positive nuclei than controls (Fig 6G and H), despite upregulation of the genes of Cyclin
661 D1 and Myc involved in cell cycle progression.
662
663 **Fig 6. No tumorigenesis was observed in double mutant kidneys.** (A) Body weight of β-catenin-GOF; Notch-
664 GOF and Vhl-LOF; β-catenin-GOF mutant mice versus controls. (B) Overview of kidneys and spleens of β-catenin-
665 GOF; Notch-GOF and Vhl-LOF; β-catenin-GOF mutant mice versus controls. (C) Kidney weight to body weight ratio
666 of β-catenin-GOF; Notch-GOF and Vhl-LOF; β-catenin-GOF mutant mice versus controls. (D) Spleen weight to
667 body weight ratio of β-catenin-GOF; Notch-GOF and Vhl-LOF; β-catenin-GOF mutant mice versus controls. (E)
668 PAS staining in β-catenin-GOF; Notch-GOF and Vhl-LOF; β-catenin-GOF mutant kidneys versus controls (in the
669 cortex and medulla) after 8 months after the doxycycline pulse. (F) PAS-stained outer part of the cortex with nuclear
670 crowding (arrowheads) in some tubules in β-catenin-GOF; Notch-GOF, but not in Vhl-LOF; β-catenin-GOF mutant
671 kidneys. (G) Immunohistochemistry for nuclear Ki67 in β-catenin-GOF; Notch-GOF and Vhl-LOF; β-catenin-GOF
672 mutant cortical kidneys versus controls after 8 months after the doxycycline pulse. (H) Quantification of Ki67-positive
673 nuclei in β-catenin-GOF; Notch-GOF and Vhl-LOF; β-catenin-GOF mutant cortical kidneys versus controls after 8
674 months after the doxycycline pulse. Data information: in A, C and D, 5 independent replicates (mice, dots) per line
675 were examined. Graphs show mean ± SD (error bars). Data passed the Shapiro-Wilk normality test (α = 0.05). The
676 ordinary one-way ANOVA followed by the Dunnett's multiple comparison to controls was performed; P-values from

677 left to right in A; 0.0001, 0.0002; ****p < 0.0001, ***p < 0.001; in C; 0.4879, 0.8354; ns: non-significant; in D; 0.0001,
678 0,0229; ****p < 0.0001, *p < 0.05. Scale bar in B, 1 cm. 20 independent replicates (all mice induced) per line were
679 examined. Scale bars in E-G, 100 µm. Nuclei are counterstained with haematoxylin. In E and G, insets are enlarged
680 on the right. 20 independent replicates (all mice induced) per line were examined. In H, three independent replicates
681 (mice, dots) with 10 technical replicates (fields per kidney) each per line were examined. Graphs show mean + SD
682 (error bars). Data passed the Shapiro-Wilk normality test (α = 0.05). The ordinary one-way ANOVA followed by the
683 Dunnett's multiple comparison to controls was performed; P-values from left to right, 0.6019, 0.9871; ns: non-
684 significant.
685
686 We neither detected accumulation of phospho-γH2AX nor p53 stabilization and the activation
687 of its downstream target p21 in nuclei of mutant kidney cells (S5A Fig). We also did not observe
688 increases in the numbers of apoptotic cells as examined by TUNEL assays (S5B Fig).
689 Together, we neither found signs of malignant transformation nor of DNA damage, senescence
690 and cell death in mutant kidneys.
691
692 **Mutant mice displayed phenotypes of CKD**
693 To confirm anemia in mutant mice, we determined the hematocrit, which significantly
694 decreased in mutant mice (Fig 7A). We also measured the concentration of erythropoietin
695 (EPO) in the blood plasma, which strongly rose in mutant mice (Fig 7B). Pathological
696 examination of the enlarged spleens of mutant mice revealed extramedullary hematopoiesis
697 by the presence of megakaryocytes (Fig 7C).
698
699 We found upregulation of tubular injury markers *Ngal*, *Kim-1* and *Gsta1* in mutant kidneys (Fig
700 7D). Moreover, the concentration of another marker of kidney injury, blood urea nitrogen
701 (BUN), was increased in mutant mice (Fig 7E). We also examined in mutant kidneys
702 expression of the inflammatory cytokine *Il1b* and of a panel of markers for myeloid lineage
703 immune cells, *Cd11b*, *Ly6c*, *Ccr2* and *Cd68*, as well as of *Icam1*, a ligand for *Cd11b*.
704 Expression of *Il1b* and *Cd11b* was upregulated in both kidney mutants, while expression of
705 *Ly6c*, *Ccr2*, *Cd68* and *Icam1* was increased in Vhl-LOF; β-catenin-GOF mutant, but not in β-

706 catenin-GOF; Notch-GOF mutant (Fig 7F). Expression of fibrotic markers, i.e. markers of
707 activated myofibroblasts, *a-sma* and *Vim*, and markers of extracellular matrix, *Fn1*, *Col1a1* and
708 *Col3a1*, was not enhanced in mutant kidneys (Fig 7G). We conclude that mutant mice exhibited
709 lethal features of CKD such as anemia as well as kidney injury and kidney inflammation. Thus,
710 we decided not to proceed with the generation of Vhl-LOF; β-catenin-GOF; Notch-GOF triple
711 mutant mice.

712

713 **Fig 7. Mutant mice displayed phenotypes of chronic kidney disease (CKD).** (A) Hematocrit of β-catenin-GOF;
714 Notch-GOF and Vhl-LOF; β-catenin-GOF mutant mice versus controls. (B) Concentration of plasma EPO in β-
715 catenin-GOF; Notch-GOF and Vhl-LOF; β-catenin-GOF mutant mice versus controls. (C) PAS staining showing
716 extramedullary hematopoiesis in spleens of β-catenin-GOF; Notch-GOF and Vhl-LOF; β-catenin-GOF mutant mice
717 versus controls. Megakaryocytes are marked by arrowheads. (D) Fold change of gene expression of kidney injury
718 markers in β-catenin-GOF; Notch-GOF and Vhl-LOF; β-catenin-GOF mutant kidneys versus controls. (E)
719 Concentration of blood urea nitrogen (BUN) in β-catenin-GOF; Notch-GOF and Vhl-LOF; β-catenin-GOF mutant
720 mice versus controls. (F) Fold change of gene expression of inflammation markers in β-catenin-GOF; Notch-GOF
721 and Vhl-LOF; β-catenin-GOF mutant kidneys versus controls. (G) Fold change of gene expression of fibrotic
722 markers of myofibroblasts and extracellular matrix in β-catenin-GOF; Notch-GOF and Vhl-LOF; β-catenin-GOF
723 mutant kidneys versus controls. Data information: in A, 5 independent replicates (mice, dots) with one technical
724 replicate each per line were examined. Graphs show mean ± SD (error bars). Data passed the Shapiro-Wilk
725 normality test ($\alpha = 0.05$). The ordinary one-way ANOVA followed by the Dunnett's multiple comparison to controls
726 was performed; P-values from left to right, 0.0001, 0.0001; ****$p < 0.0001$. In B, 5 independent replicates (mice,
727 dots) in technical triplicates per line were examined. Graphs show mean ± SD (error bars). No statistical test was
728 performed because of high inter-mouse variance. However, increase trends were observed. Scale bars in C, 100
729 μm. Nuclei are counterstained with haematoxylin. An undisrupted follicular B-cell compartment in the white pulp in
730 controls is marked by white lines. Insets are enlarged on the right. Three independent replicates per line were
731 examined. In D, three independent replicates (mice, dots) in technical triplicates were examined. Graphs show
732 mean + SD (error bars). No statistical test was performed because of high inter-mouse variance. However, increase
733 trends were observed. In E, 5 independent replicates (mice, dots) with one technical replicate each per line were
734 examined. Graphs show mean ± SD (error bars). Data passed the Shapiro-Wilk normality test ($\alpha = 0.05$). The
735 ordinary one-way ANOVA followed by the Dunnett's multiple comparison to controls was performed; P-values from
736 left to right, 0.0109, 0.0888; *$p < 0.05$, ns: non-significant. Although the difference in average concentration of BUN
737 between the Vhl-LOF; β-catenin-GOF mutant mice and controls was non-significant ($p < 0.05$), an increase trend

was observed. In F and G, three independent replicates (mice, dots) in technical triplicates were examined. Graphs show mean + SD (error bars). No statistical test was performed because of high inter-mouse variance. However, increase trends were observed in F and no increase trends were observed in G.

742 # Discussion

743 **Tubular organoid cultures from adult mouse kidneys enrich for stem/progenitor cells**
744 **with active Wnt and Notch signaling**

745 We have established robust organoid cultures from single epithelial cells from adult mouse
746 kidneys and have examined their cellular components and stem cell-associated signaling
747 systems at protein levels by deep bulk proteomic and phosphoproteomic analyses. These
748 approaches represent so far the most thorough recording of important proteins and
749 phosphorylation sites performed in kidney organoids. We found that the organoids shared
750 proteome and phosphoprotome patterns with adult kidney tubular epithelia to a great extent
751 and were phenotypically stable over long-term passages. Proteomic analysis revealed
752 enhanced proliferation and upregulation of stem cell-associated Wnt, Notch and Yap signaling
753 in the organoids, which indicated the recapitulation of kidney renewal response, similar to mice
754 upon kidney injury (3–6,40). Functionally, Wnt was crucial for both self-renewal and
755 differentiation of organoid cells. Despite high coverage, we were not able to detect important
756 proteins such as collecting duct-specific Aquaporin 3, which we detected using other
757 techniques. To characterize the organoids more thoroughly, single cell RNA sequencing
758 should be performed in the future. Once optimized, single cell proteomics will remarkably
759 improve a global analysis of protein levels in individual organoid cells (41). We did not examine
760 the functional importance of phosphorylation patterns of detected proteins, because this went
761 beyond the scope of our manuscript. However, we believe that the phosphoproteomic data set
762 holds a lot of interesting information for other researchers regarding signaling systems of
763 kidney stem cells. In future studies, the or-ganoid model will assist analyses of Wnt- and Notch-
764 dependent self-renewal of marker-sorted kidney stem/progenitor cell populations, which will
765 then possibly link these cells with their malignant counterparts, for instance, with the ones
766 identified by our group (14).

767

768 **Our findings in genetic models of adult mouse kidneys challenge the current**
769 **understanding of the involvement of stem cell-associated Wnt and Notch signaling in**
770 **development of human ccRCC**
771 Surprisingly, the two types of double kidney mutants in mice, i.e. β-cat-GOF with Notch-GOF
772 or with Vhl-LOF, did not produce tumors or premalignant lesions. This occurred despite a
773 rational hypothesis on the involvement of Wnt-high and Notch-high stem cells in development
774 of human ccRCC, and despite using a well-designed genetic system to target adult proximal
775 tubular epithelial cells, the cells of tumor origin. However, the mouse mutants displayed strong
776 fatal phenotypes that resembled CKD (42,43). The significance of the interplay of Wnt and
777 Notch as well as of Wnt and Vhl loss in development of CKD has not previously been defined.
778
779 Wnt hyperactivation using embryonic Cres in other mouse models resulted in development of
780 polycystic kidney disease (44,45). Wnt upregulation in tubular cells or podocytes of adult
781 mouse kidneys contributed to either tubular and glomerular damage and tubule-interstitial
782 inflammation or to albuminuria, indicating CKD (46,47). In another mouse model, adult kidneys
783 with Notch hyperactivation exhibited CKD with pronounced tubular degeneration and dilation
784 as well as tubule-interstitial inflammation and fibrosis (48). By single cell RNA sequencing,
785 plasticity of collecting duct cells in the mouse kidney was revealed, which upon Notch
786 upregulation was disturbed and correlated with metabolic acidosis observed in CKD patients
787 (49). Moreover, in numerous rodent models of kidney injury, transient activation of Wnt and
788 Notch accelerated regeneration, but sustained activation promoted maladaptative behaviors
789 and CKD progression (50). Of note, Notch upregulation in mouse kidneys in another study led
790 to development of both CKD and a relatively rare papillary kidney cancer, and this process
791 was accelerated by kidney injury (51). In addition, the authors found a correlation of a kidney
792 injury episode with subsequent occurrence of papillary cancer but not ccRCC in patients.
793
794 Lack of fibrosis in our models might suggest that mutant mice have not yet progressed to end-
795 stage CKD. Remarkably, mutant mice produced additional features of CKD, which so far have

796 not been reported in other studies that examined hyperactivation of either Wnt or Notch in adult
797 mouse kidneys (47,48). Mutant mice exhibited dramatic anemic phenotypes, despite strong
798 increases in plasma erythropoietin levels. This compensative positive feedback on EPO
799 production suggests a mechanism of anemia development downstream of EPO supply.
800 Inflammation that we detected in mutant mice could be a driver of anemia in CKD, either
801 directly through inhibition of EPO-mediated erythropoiesis or indirectly via disrupted iron
802 regulation that limits hemoglobin synthesis in erythroid cells in the bone marrow (43).
803 Moreover, we documented extramedullary hematopoiesis in enlarged spleens of mutant mice,
804 which may be induced in response to anemia and involves expansion and differentiation of
805 erythroid, myeloid and platelet precursors into effector cells outside the bone marrow (52).
806
807 We suspect that focal recombination in adult kidney epithelial cells in mice through decreased
808 doses of doxycycline might support tumor development by overcoming severe CKD
809 phenotypes (53,54). Thus, our reproducible and penetrant genetic system can be used for
810 further studies of downstream effectors of Wnt and Notch signaling in the context of the
811 pathobiology of kidney stem/progenitor cells, irrespective whether this results in CKD or
812 tumors. We conclude that the organoid model displayed responses of kidney stem cells that
813 resulted in high self-renewal, in contrast to the genetic mouse mutants that produced CKD
814 phenotypes, but no elevated proliferation and tumors.

Author Contributions

Conceptualization, A.M., A.F., P.M. and W.B.; investigation, A.M., O.P., S.K. and S.J.; formal analysis and visualization, A.M., O.P., S.K. and A.S.; writing, A.M., L.C.P. and W.B.; supervision, P.M. and W.B.

Acknowledgments

We would like to thank Prof. Dr. med. Wolfgang Schneider and Dr. med. Ann-Christin von Brünneck from the Institute of Pathology at the Charité-Medical University Berlin for the histopathological examinations. Further, we thank Prof. Dr. med. Friedrich Luft from the Experimental and Clinical Research Center (ECRC) in Berlin for giving us important experimental suggestions. We would also like to acknowledge Dr. Bart Spee from the Faculty of Veterinary Medicine at the Utrecht University for his valuable comments on the manuscript.

Funding

A.M. and A.F. were funded in part by the Urological Research Foundation (Stiftung Urologische Forschung) in Berlin.

Data Availability Statement

The mass spectrometry proteomics and phosphoproteomics data were deposited to the ProteomeXchange Consortium via the PRIDE partner depository (55) with the dataset identifier PXD023491.

838 # References

839 1. Grigoryan T, Wend P, Klaus A, Birchmeier W. Deciphering the function of canonical Wnt signals in
840 development and disease: conditional loss- and gain-of-function mutations of -catenin in mice. Genes Dev
841 [Internet]. 2008 Sep 1;22(17):2308–41. Available from:
842 http://genesdev.cshlp.org/cgi/doi/10.1101/gad.1686208
843 2. Koch U, Lehal R, Radtke F. Stem cells living with a Notch. Development [Internet]. 2013 Feb
844 15;140(4):689–704. Available from: http://dev.biologists.org/cgi/doi/10.1242/dev.080614
845 3. Kang HM, Huang S, Reidy K, Han SH, Chinga F, Susztak K. Sox9-Positive Progenitor Cells Play a Key
846 Role in Renal Tubule Epithelial Regeneration in Mice. Cell Rep [Internet]. 2016 Feb;14(4):861–71.
847 Available from: https://linkinghub.elsevier.com/retrieve/pii/S2211124715015259
848 4. Rinkevich Y, Montoro DT, Contreras-Trujillo H, Harari-Steinberg O, Newman AM, Tsai JM, et al. In Vivo
849 Clonal Analysis Reveals Lineage-Restricted Progenitor Characteristics in Mammalian Kidney
850 Development, Maintenance, and Regeneration. Cell Rep [Internet]. 2014 May;7(4):1270–83. Available
851 from: https://linkinghub.elsevier.com/retrieve/pii/S2211124714003052
852 5. Chen J, Chen J-K, Conway EM, Harris RC. Survivin Mediates Renal Proximal Tubule Recovery from AKI.
853 J Am Soc Nephrol [Internet]. 2013 Dec;24(12):2023–33. Available from:
854 https://jasn.asnjournals.org/lookup/doi/10.1681/ASN.2013010076
855 6. Zhou D, Li Y, Lin L, Zhou L, Igarashi P, Liu Y. Tubule-specific ablation of endogenous β-catenin
856 aggravates acute kidney injury in mice. Kidney Int [Internet]. 2012 Sep;82(5):537–47. Available from:
857 https://linkinghub.elsevier.com/retrieve/pii/S0085253815555956
858 7. Lancaster MA, Knoblich JA. Organogenesis in a dish: Modeling development and disease using organoid
859 technologies. Science (80-) [Internet]. 2014 Jul 18;345(6194):1247125–1247125. Available from:
860 https://www.sciencemag.org/lookup/doi/10.1126/science.1247125
861 8. Schutgens F, Clevers H. Human Organoids: Tools for Understanding Biology and Treating Diseases.
862 Annu Rev Pathol Mech Dis [Internet]. 2020 Jan 24;15(1):211–34. Available from:
863 https://www.annualreviews.org/doi/10.1146/annurev-pathmechdis-012419-032611
864 9. Grassi L, Alfonsi R, Francescangeli F, Signore M, De Angelis ML, Addario A, et al. Organoids as a new
865 model for improving regenerative medicine and cancer personalized therapy in renal diseases. Cell Death
866 Dis [Internet]. 2019 Mar 27;10(3):201. Available from: http://www.nature.com/articles/s41419-019-1453-0
867 10. Schutgens F, Rookmaaker MB, Margaritis T, Rios A, Ammerlaan C, Jansen J, et al. Tubuloids derived
868 from human adult kidney and urine for personalized disease modeling. Nat Biotechnol [Internet]. 2019
869 Mar 4;37(3):303–13. Available from: http://www.nature.com/articles/s41587-019-0048-8
870 11. Hsieh JJ, Purdue MP, Signoretti S, Swanton C, Albiges L, Schmidinger M, et al. Renal cell carcinoma.

871 Nat Rev Dis Prim [Internet]. 2017 Dec 21;3(1):17009. Available from:
872 http://www.nature.com/articles/nrdp20179
873 12. Gossage L, Eisen T, Maher ER. VHL, the story of a tumour suppressor gene. Nat Rev Cancer [Internet].
874 2015 Jan 23;15(1):55–64. Available from: http://www.nature.com/articles/nrc3844
875 13. Hou W, Ji Z. Generation of autochthonous mouse models of clear cell renal cell carcinoma: mouse
876 models of renal cell carcinoma. Exp Mol Med [Internet]. 2018 Apr 13;50(4):30. Available from:
877 http://www.nature.com/articles/s12276-018-0059-4
878 14. Fendler A, Bauer D, Busch J, Jung K, Wulf-Goldenberg A, Kunz S, et al. Inhibiting WNT and NOTCH in
879 renal cancer stem cells and the implications for human patients. Nat Commun. 2020 Dec 17;11(1):929.
880 15. Cole AM, Ridgway RA, Derkits SE, Parry L, Barker N, Clevers H, et al. p21 loss blocks senescence
881 following Apc loss and provokes tumourigenesis in the renal but not the intestinal epithelium. EMBO Mol
882 Med [Internet]. 2010 Nov 26;2(11):472–86. Available from:
883 https://onlinelibrary.wiley.com/doi/10.1002/emmm.201000101
884 16. Sansom OJ, Griffiths DFR, Reed KR, Winton DJ, Clarke AR. Apc deficiency predisposes to renal
885 carcinoma in the mouse. Oncogene [Internet]. 2005 Dec 22;24(55):8205–10. Available from:
886 http://www.nature.com/articles/1208956
887 17. Clark PE, Polosukhina D, Love H, Correa H, Coffin C, Perlman EJ, et al. β-Catenin and K-RAS Synergize
888 to Form Primitive Renal Epithelial Tumors with Features of Epithelial Wilms' Tumors. Am J Pathol
889 [Internet]. 2011 Dec;179(6):3045–55. Available from:
890 https://linkinghub.elsevier.com/retrieve/pii/S000294401100808X
891 18. Sansom OJ, Meniel V, Wilkins JA, Cole AM, Oien KA, Marsh V, et al. Loss of Apc allows phenotypic
892 manifestation of the transforming properties of an endogenous K-ras oncogene in vivo. Proc Natl Acad
893 Sci [Internet]. 2006 Sep 19;103(38):14122–7. Available from:
894 http://www.pnas.org/cgi/doi/10.1073/pnas.0604130103
895 19. Bhagat TD, Zou Y, Huang S, Park J, Palmer MB, Hu C, et al. Notch Pathway Is Activated via Genetic and
896 Epigenetic Alterations and Is a Therapeutic Target in Clear Cell Renal Cancer. J Biol Chem [Internet].
897 2017 Jan;292(3):837–46. Available from: https://linkinghub.elsevier.com/retrieve/pii/S0021925820402649
898 20. Johansson E, Rönö B, Johansson M, Lindgren D, Möller C, Axelson H, et al. Simultaneous targeted
899 activation of Notch1 and Vhl-disruption in the kidney proximal epithelial tubular cells in mice. Sci Rep
900 [Internet]. 2016 Aug 5;6(1):30739. Available from: http://www.nature.com/articles/srep30739
901 21. Zhu L, Finkelstein D, Gao C, Shi L, Wang Y, López-Terrada D, et al. Multi-organ Mapping of Cancer Risk.
902 Cell [Internet]. 2016 Aug;166(5):1132-1146.e7. Available from:
903 https://linkinghub.elsevier.com/retrieve/pii/S0092867416309953
904 22. Schönig K, Schwenk F, Rajewsky K, Bujard H. Stringent doxycycline dependent control of CRE

905 recombinase in vivo. Nucleic Acids Res. 2002;
906 23. Harada N. Intestinal polyposis in mice with a dominant stable mutation of the beta -catenin gene. EMBO J
907 [Internet]. 1999 Nov 1;18(21):5931–42. Available from:
908 http://emboj.embopress.org/cgi/doi/10.1093/emboj/18.21.5931
909 24. Murtaugh LC, Stanger BZ, Kwan KM, Melton DA. Notch signaling controls multiple steps of pancreatic
910 differentiation. Proc Natl Acad Sci [Internet]. 2003 Dec 9;100(25):14920–5. Available from:
911 http://www.pnas.org/cgi/doi/10.1073/pnas.2436557100
912 25. Soriano P. Generalized lacZ expression with the ROSA26 Cre reporter strain. Nat Genet [Internet]. 1999
913 Jan;21(1):70–1. Available from: http://www.nature.com/articles/ng0199_70
914 26. Traykova-Brauch M, Schönig K, Greiner O, Miloud T, Jauch A, Bode M, et al. An efficient and versatile
915 system for acute and chronic modulation of renal tubular function in transgenic mice. Nat Med. 2008 Sep
916 24;14(9):979–84.
917 27. Haase VH, Glickman JN, Socolovsky M, Jaenisch R. Vascular tumors in livers with targeted inactivation
918 of the von Hippel-Lindau tumor suppressor. Proc Natl Acad Sci [Internet]. 2001 Feb 13;98(4):1583–8.
919 Available from: http://www.pnas.org/cgi/doi/10.1073/pnas.98.4.1583
920 28. Holmberg FE, Seidelin JB, Yin X, Mead BE, Tong Z, Li Y, et al. Culturing human intestinal stem cells for
921 regenerative applications in the treatment of inflammatory bowel disease. EMBO Mol Med [Internet]. 2017
922 May 10;9(5):558–70. Available from: https://onlinelibrary.wiley.com/doi/abs/10.15252/emmm.201607260
923 29. Sato T, Stange DE, Ferrante M, Vries RGJ, van Es JH, van den Brink S, et al. Long-term Expansion of
924 Epithelial Organoids From Human Colon, Adenoma, Adenocarcinoma, and Barrett's Epithelium.
925 Gastroenterology [Internet]. 2011 Nov;141(5):1762–72. Available from:
926 https://linkinghub.elsevier.com/retrieve/pii/S0016508511011085
927 30. Cato ACB, Nestl A, Mink S. Rapid Actions of Steroid Receptors in Cellular Signaling Pathways. Sci Signal
928 [Internet]. 2002 Jun 25;2002(138):re9–re9. Available from:
929 https://stke.sciencemag.org/lookup/doi/10.1126/stke.2002.138.re9
930 31. Sorrentino G, Ruggeri N, Zannini A, Ingallina E, Bertolio R, Marotta C, et al. Glucocorticoid receptor
931 signalling activates YAP in breast cancer. Nat Commun [Internet]. 2017 Apr 19;8(1):14073. Available
932 from: http://www.nature.com/articles/ncomms14073
933 32. Mertins P, Tang LC, Krug K, Clark DJ, Gritsenko MA, Chen L, et al. Reproducible workflow for
934 multiplexed deep-scale proteome and phosphoproteome analysis of tumor tissues by liquid
935 chromatography–mass spectrometry. Nat Protoc [Internet]. 2018 Jul 9;13(7):1632–61. Available from:
936 http://www.nature.com/articles/s41596-018-0006-9
937 33. Cox J, Mann M. MaxQuant enables high peptide identification rates, individualized p.p.b.-range mass
938 accuracies and proteome-wide protein quantification. Nat Biotechnol [Internet]. 2008 Dec

939 30;26(12):1367–72. Available from: http://www.nature.com/articles/nbt.1511
940 34. Ritchie ME, Phipson B, Wu D, Hu Y, Law CW, Shi W, et al. limma powers differential expression analyses
941 for RNA-sequencing and microarray studies. Nucleic Acids Res [Internet]. 2015 Apr 20;43(7):e47–e47.
942 Available from: http://academic.oup.com/nar/article/43/7/e47/2414268/limma-powers-differential-
943 expression-analyses-for
944 35. Herbst A, Jurinovic V, Krebs S, Thieme SE, Blum H, Göke B, et al. Comprehensive analysis of β-catenin
945 target genes in colorectal carcinoma cell lines with deregulated Wnt/β-catenin signaling. BMC Genomics
946 [Internet]. 2014;15(1):74. Available from: http://bmcgenomics.biomedcentral.com/articles/10.1186/1471-
947 2164-15-74
948 36. Zanconato F, Forcato M, Battilana G, Azzolin L, Quaranta E, Bodega B, et al. Genome-wide association
949 between YAP/TAZ/TEAD and AP-1 at enhancers drives oncogenic growth. Nat Cell Biol [Internet]. 2015
950 Sep 10;17(9):1218–27. Available from: http://www.nature.com/articles/ncb3216
951 37. Rankin EB, Tomaszewski JE, Haase VH. Renal Cyst Development in Mice with Conditional Inactivation of
952 the von Hippel-Lindau Tumor Suppressor. Cancer Res [Internet]. 2006 Mar 1;66(5):2576–83. Available
953 from: http://cancerres.aacrjournals.org/lookup/doi/10.1158/0008-5472.CAN-05-3241
954 38. Nielsen R, Christensen EI, Birn H. Megalin and cubilin in proximal tubule protein reabsorption: from
955 experimental models to human disease. Kidney Int [Internet]. 2016 Jan;89(1):58–67. Available from:
956 https://linkinghub.elsevier.com/retrieve/pii/S0085253815000551
957 39. Fang L, Zhu Q, Neuenschwander M, Specker E, Wulf-Goldenberg A, Weis WI, et al. A Small-Molecule
958 Antagonist of the β-Catenin/TCF4 Interaction Blocks the Self-Renewal of Cancer Stem Cells and
959 Suppresses Tumorigenesis. Cancer Res [Internet]. 2016 Feb 15;76(4):891–901. Available from:
960 http://cancerres.aacrjournals.org/lookup/doi/10.1158/0008-5472.CAN-15-1519
961 40. Chen J, You H, Li Y, Xu Y, He Q, Harris RC. EGF Receptor–Dependent YAP Activation Is Important for
962 Renal Recovery from AKI. J Am Soc Nephrol [Internet]. 2018 Sep;29(9):2372–85. Available from:
963 https://jasn.asnjournals.org/lookup/doi/10.1681/ASN.2017121272
964 41. Marx V. A dream of single-cell proteomics. Nat Methods [Internet]. 2019 Sep 12;16(9):809–12. Available
965 from: http://www.nature.com/articles/s41592-019-0540-6
966 42. Ferenbach DA, Bonventre J V. Mechanisms of maladaptive repair after AKI leading to accelerated kidney
967 ageing and CKD. Nat Rev Nephrol [Internet]. 2015 May 3;11(5):264–76. Available from:
968 http://www.nature.com/articles/nrneph.2015.3
969 43. Koury MJ, Haase VH. Anaemia in kidney disease: harnessing hypoxia responses for therapy. Nat Rev
970 Nephrol [Internet]. 2015 Jul 9;11(7):394–410. Available from:
971 http://www.nature.com/articles/nrneph.2015.82
972 44. Qian C-N, Knol J, Igarashi P, Lin F, Zylstra U, Teh BT, et al. Cystic Renal Neoplasia Following

973 Conditional Inactivation of Apc in Mouse Renal Tubular Epithelium. J Biol Chem [Internet]. 2005
974 Feb;280(5):3938–45. Available from: https://linkinghub.elsevier.com/retrieve/pii/S0021925820762666
975 45. Saadi-Kheddouci S, Berrebi D, Romagnolo B, Cluzeaud F, Peuchmaur M, Kahn A, et al. Early
976 development of polycystic kidney disease in transgenic mice expressing an activated mutant of the β-
977 catenin gene. Oncogene [Internet]. 2001 Sep 9;20(42):5972–81. Available from:
978 http://www.nature.com/articles/1204825
979 46. Kato H, Gruenwald A, Suh JH, Miner JH, Barisoni-Thomas L, Taketo MM, et al. Wnt/β-Catenin Pathway
980 in Podocytes Integrates Cell Adhesion, Differentiation, and Survival. J Biol Chem [Internet]. 2011
981 Jul;286(29):26003–15. Available from: https://linkinghub.elsevier.com/retrieve/pii/S0021925819485876
982 47. Wong DWL, Yiu WH, Chan KW, Li Y, Li B, Lok SWY, et al. Activated renal tubular Wnt/β-catenin signaling
983 triggers renal inflammation during overload proteinuria. Kidney Int [Internet]. 2018 Jun;93(6):1367–83.
984 Available from: https://linkinghub.elsevier.com/retrieve/pii/S0085253818300838
985 48. Bielesz B, Sirin Y, Si H, Niranjan T, Gruenwald A, Ahn S, et al. Epithelial Notch signaling regulates
986 interstitial fibrosis development in the kidneys of mice and humans. J Clin Invest [Internet]. 2010 Nov
987 1;120(11):4040–54. Available from: http://www.jci.org/articles/view/43025
988 49. Park J, Shrestha R, Qiu C, Kondo A, Huang S, Werth M, et al. Single-cell transcriptomics of the mouse
989 kidney reveals potential cellular targets of kidney disease. Science (80-) [Internet]. 2018 May
990 18;360(6390):758–63. Available from: https://www.sciencemag.org/lookup/doi/10.1126/science.aar2131
991 50. Edeling M, Ragi G, Huang S, Pavenstädt H, Susztak K. Developmental signalling pathways in renal
992 fibrosis: the roles of Notch, Wnt and Hedgehog. Nat Rev Nephrol [Internet]. 2016 Jul 3;12(7):426–39.
993 Available from: http://www.nature.com/articles/nrneph.2016.54
994 51. Peired AJ, Antonelli G, Angelotti ML, Allinovi M, Guzzi F, Sisti A, et al. Acute kidney injury promotes
995 development of papillary renal cell adenoma and carcinoma from renal progenitor cells. Sci Transl Med.
996 2020;
997 52. Chiu S-C, Liu H-H, Chen C-L, Chen P-R, Liu M-C, Lin S-Z, et al. Extramedullary Hematopoiesis (EMH) in
998 Laboratory Animals: Offering an Insight into Stem Cell Research. Cell Transplant [Internet]. 2015
999 Mar;24(3):349–66. Available from: http://journals.sagepub.com/doi/full/10.3727/096368915X686850
1000 53. Carter P, Schnell U, Chaney C, Tong B, Pan X, Ye J, et al. Deletion of Lats1/2 in adult kidney epithelia
1001 leads to renal cell carcinoma. J Clin Invest [Internet]. 2021 Jun 1;131(11). Available from:
1002 https://www.jci.org/articles/view/144108
1003 54. Harada N, Miyoshi H, Murai N, Oshima H, Tamai Y, Oshima M, et al. Lack of tumorigenesis in the mouse
1004 liver after adenovirus-mediated expression of a dominant stable mutant of β-catenin. Cancer Res. 2002;
1005 55. Perez-Riverol Y, Csordas A, Bai J, Bernal-Llinares M, Hewapathirana S, Kundu DJ, et al. The PRIDE
1006 database and related tools and resources in 2019: improving support for quantification data. Nucleic

1007 Acids Res [Internet]. 2019 Jan 8;47(D1):D442–50. Available from:
1008 https://academic.oup.com/nar/article/47/D1/D442/5160986
1009

1010 ## Supporting Information

1011 S1 Figure: Long-term culture of kidney organoids and establishing kidney organoids of different
1012 mouse backgrounds.

1013 S2 Figure: Yap signaling is upregulated in kidney organoids.

1014 S3 Figure: Markers of tubular epithelial cells are expressed in 3D reconstructed kidney
1015 organoids.

1016 S4 Figure: Kidney organoids display tubular epithelial polarity and complexity.

1017 S5 Figure: No DNA damage, growth arrest or senescence and increased apoptosis was
1018 observed in mutant kidneys.

1019 S1 Video: Markers of tubular epithelial cells are expressed in 3D reconstructed kidney
1020 organoids.

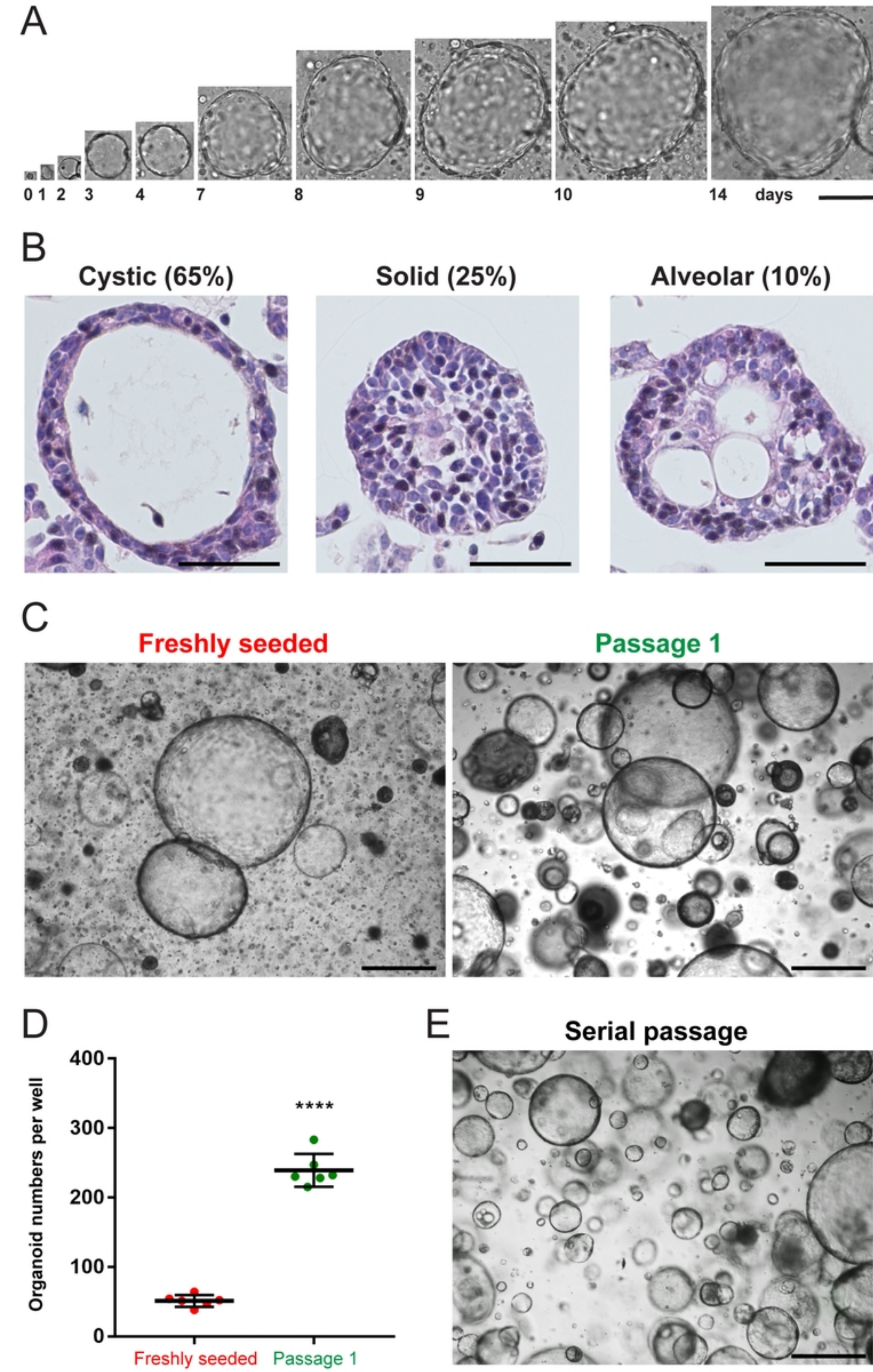
A
0 1 2 3 4 7 8 9 10 14 days
B
Cystic (65%)
Solid (25%)
Alveolar (10%)
C
Freshly seeded
Passage 1
D
Organoid numbers per well
400
300
200
100
0
****
Freshly seeded
Passage 1
E
Serial passage

Fig 1

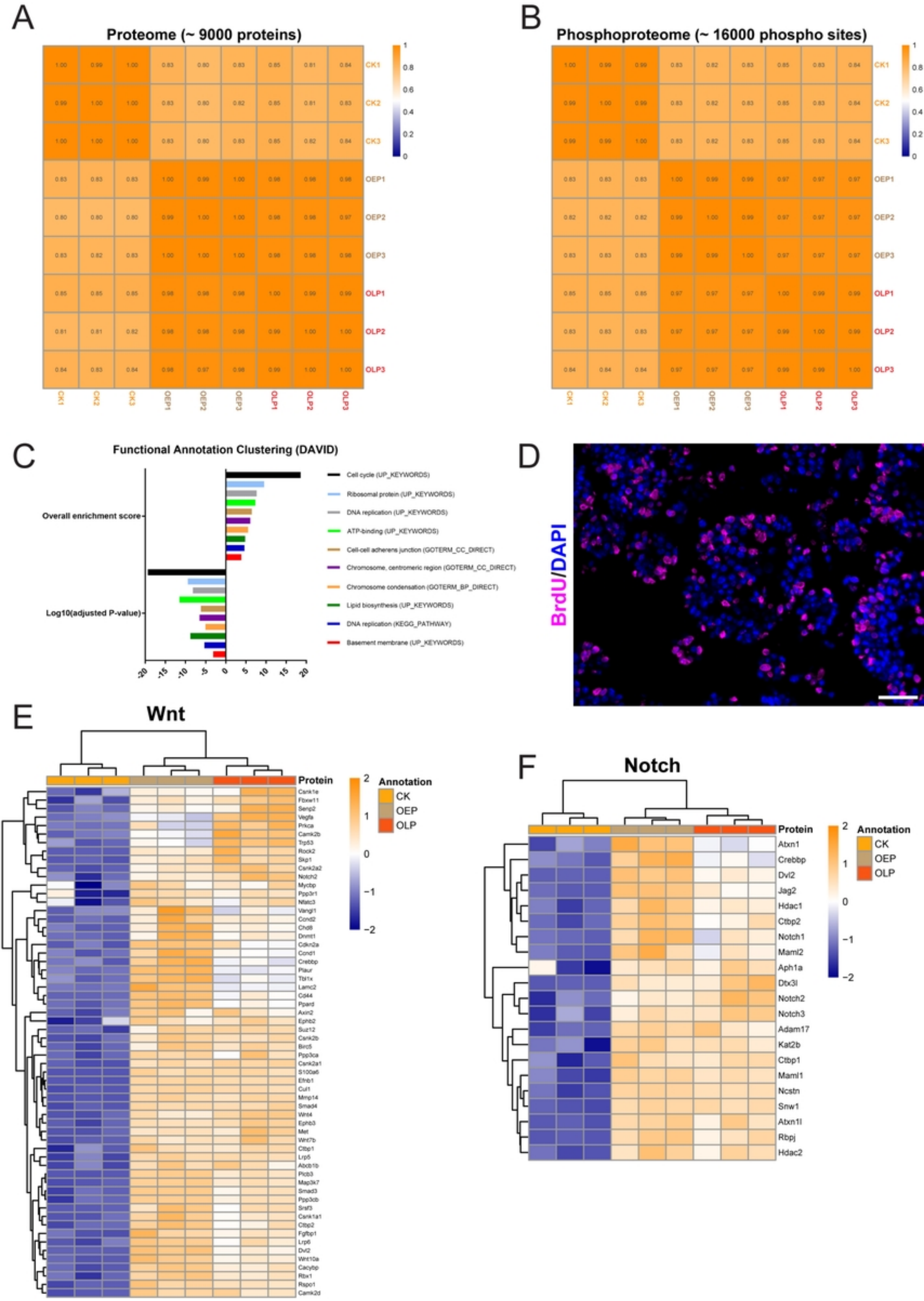
A
Proteome (~ 9000 proteins)
CK1
CK2
CK3
OEP1
OEP2
OEP3
OLP1
OLP2
OLP3
B
Phosphoproteome (~ 16000 phospho sites)
C
Functional Annotation Clustering (DAVID)
Overall enrichment score
Log10(adjusted P-value)
Cell cycle (UP_KEYWORDS)
Ribosomal protein (UP_KEYWORDS)
DNA replication (UP_KEYWORDS)
ATP-binding (UP_KEYWORDS)
Cell-cell adherens junction (GOTERM_CC_DIRECT)
Chromosome, centromeric region (GOTERM_CC_DIRECT)
Chromosome condensation (GOTERM_BP_DIRECT)
Lipid biosynthesis (UP_KEYWORDS)
DNA replication (KEGG_PATHWAY)
Basement membrane (UP_KEYWORDS)
D
BrdU/DAPI
E
Wnt
Protein
Annotation
CK
OEP
OLP
F
Notch
Protein
Annotation
CK
OEP
OLP
Abxn1
Crebbp
Dvl2
Jag2
Hdac1
Ctbp2
Notch1
Maml2
Aph1a
Dtx3l
Notch2
Notch3
Adam17
Kat2b
Ctbp1
Maml1
Ncstn
Snw1
Abxn1l
Rbpj
Hdac2

Fig 2

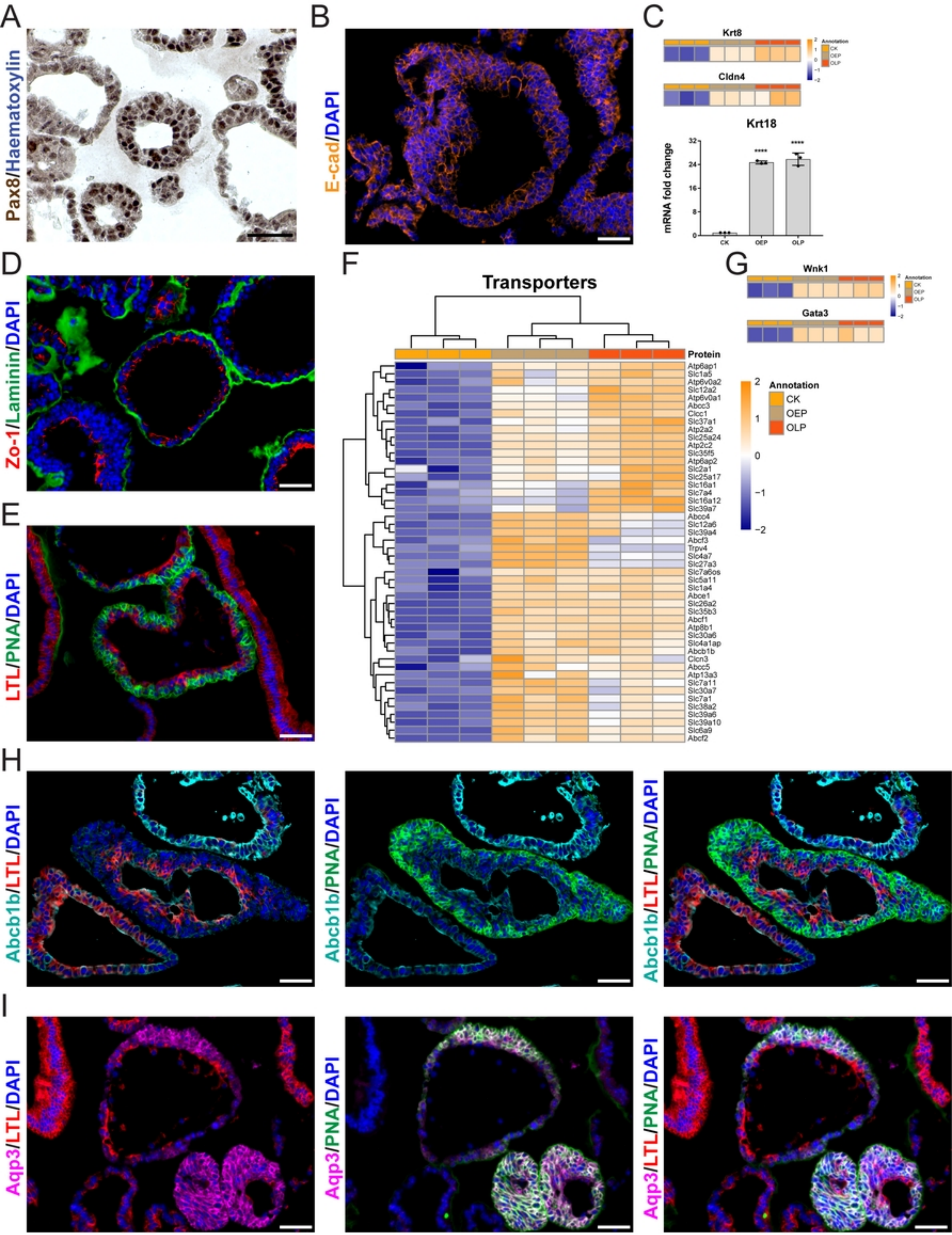
A
Pax8/Haematoxylin
B
E-cad/DAPI
C
Krt8
Cldn4
Krt18
mRNA fold change
CK
OEP
OLP
D
Zo-1/Laminin/DAPI
E
LTL/PNA/DAPI
F
Transporters
Protein
Annotation
CK
OEP
OLP
G
Wnk1
Gata3
H
Abcb1b/LTL/DAPI
Abcb1b/PNA/DAPI
Abcb1b/LTL/PNA/DAPI
I
Aqp3/LTL/DAPI
Aqp3/PNA/DAPI
Aqp3/LTL/PNA/DAPI

Fig 3

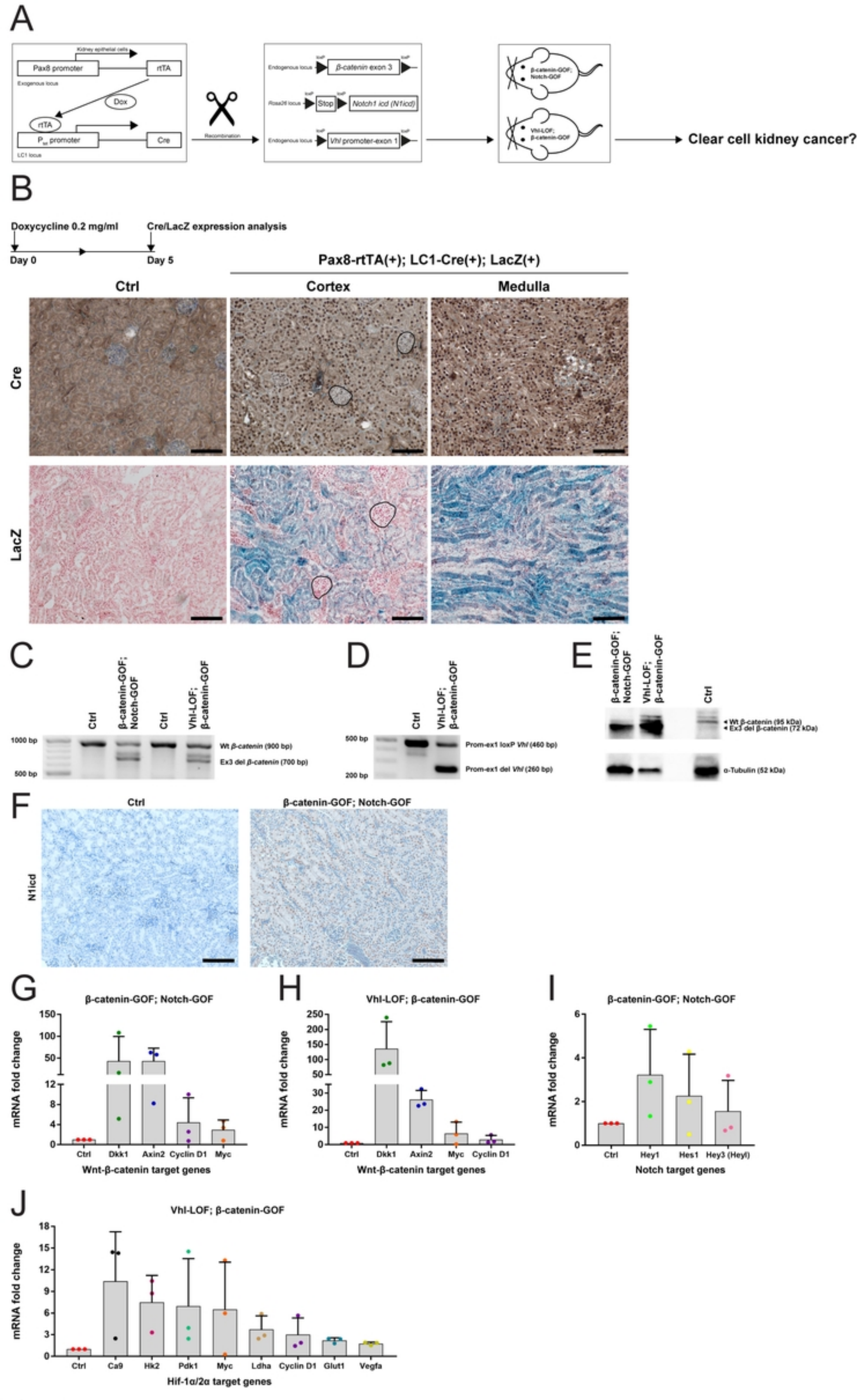
A
Kidney epithelial cells
Pax8 promoter
rtTA
Exogenous locus
Dox
rtTA
Cre
LC1 locus
Recombination
Endogenous locus
β-catenin exon 3
Rosa26 locus
Stop
Notch1 icd (N1icd)
Endogenous locus
Vhl promoter-exon 1
β-catenin-GOF; Notch-GOF
Vhl-LOF; β-catenin-GOF
Clear cell kidney cancer?
B
Doxycycline 0.2 mg/ml
Cre/LacZ expression analysis
Day 0
Day 5
Pax8-rtTA(+); LC1-Cre(+); LacZ(+)
Ctrl
Cortex
Medulla
Cre
LacZ
C
Ctrl
β-catenin-GOF; Notch-GOF
Ctrl
Vhl-LOF; β-catenin-GOF
1000 bp
500 bp
Wt β-catenin (900 bp)
Ex3 del β-catenin (700 bp)
D
Ctrl
Vhl-LOF; β-catenin-GOF
500 bp
200 bp
Prom-ex1 loxP Vhl (460 bp)
Prom-ex1 del Vhl (260 bp)
E
β-catenin-GOF; Notch-GOF
Vhl-LOF; β-catenin-GOF
Ctrl
Wt β-catenin (95 kDa)
Ex3 del β-catenin (72 kDa)
α-Tubulin (52 kDa)
F
Ctrl
β-catenin-GOF; Notch-GOF
N1icd
G
β-catenin-GOF; Notch-GOF
mRNA fold change
Ctrl
Dkk1
Axin2
Cyclin D1
Myc
Wnt-β-catenin target genes
H
Vhl-LOF; β-catenin-GOF
mRNA fold change
Ctrl
Dkk1
Axin2
Myc
Cyclin D1
Wnt-β-catenin target genes
I
β-catenin-GOF; Notch-GOF
mRNA fold change
Ctrl
Hey1
Hes1
Hey3 (Heyl)
Notch target genes
J
Vhl-LOF; β-catenin-GOF
mRNA fold change
Ctrl
Ca9
Hk2
Pdk1
Myc
Ldha
Cyclin D1
Glut1
Vegfa
Hif-1α/2α target genes

Fig 5

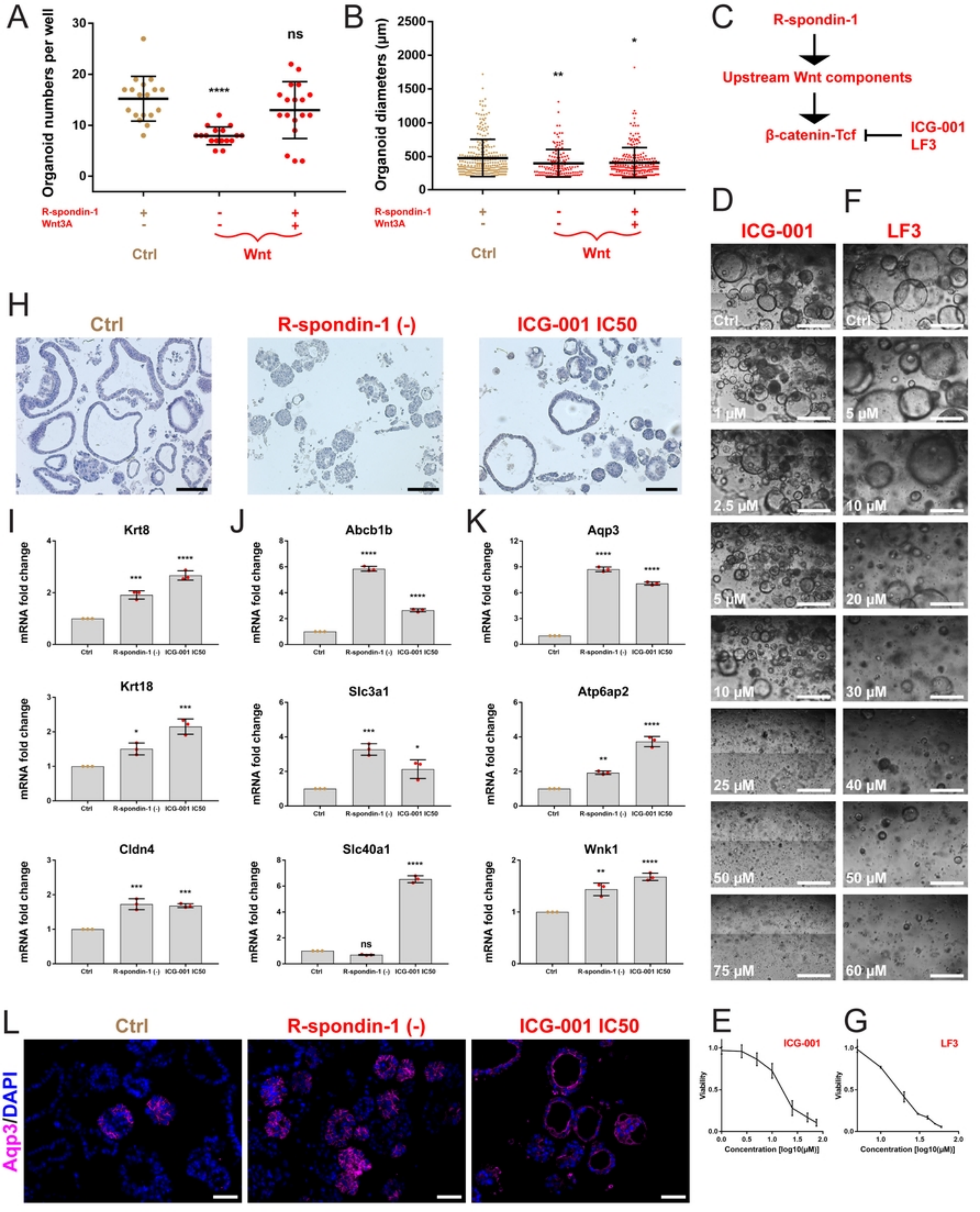
A
Organoid numbers per well
ns
****
R-spondin-1
Wnt3A
Ctrl
Wnt
B
Organoid diameters (μm)
**
*
R-spondin-1
Wnt3A
Ctrl
Wnt
C
R-spondin-1
Upstream Wnt components
β-catenin-Tcf
ICG-001
LF3
D
ICG-001
F
LF3
Ctrl
1 μM
2.5 μM
5 μM
10 μM
25 μM
50 μM
75 μM
5 μM
10 μM
20 μM
30 μM
40 μM
50 μM
60 μM
H
Ctrl
R-spondin-1 (-)
ICG-001 IC50
I
Krt8
Krt18
Cldn4
J
Abcb1b
Slc3a1
Slc40a1
K
Aqp3
Atp6ap2
Wnk1
mRNA fold change
Ctrl
R-spondin-1 (-)
ICG-001 IC50
L
Ctrl
R-spondin-1 (-)
ICG-001 IC50
Aqp3/DAPI
E
ICG-001
G
LF3
Viability
Concentration [log10(μM)]

Fig 4

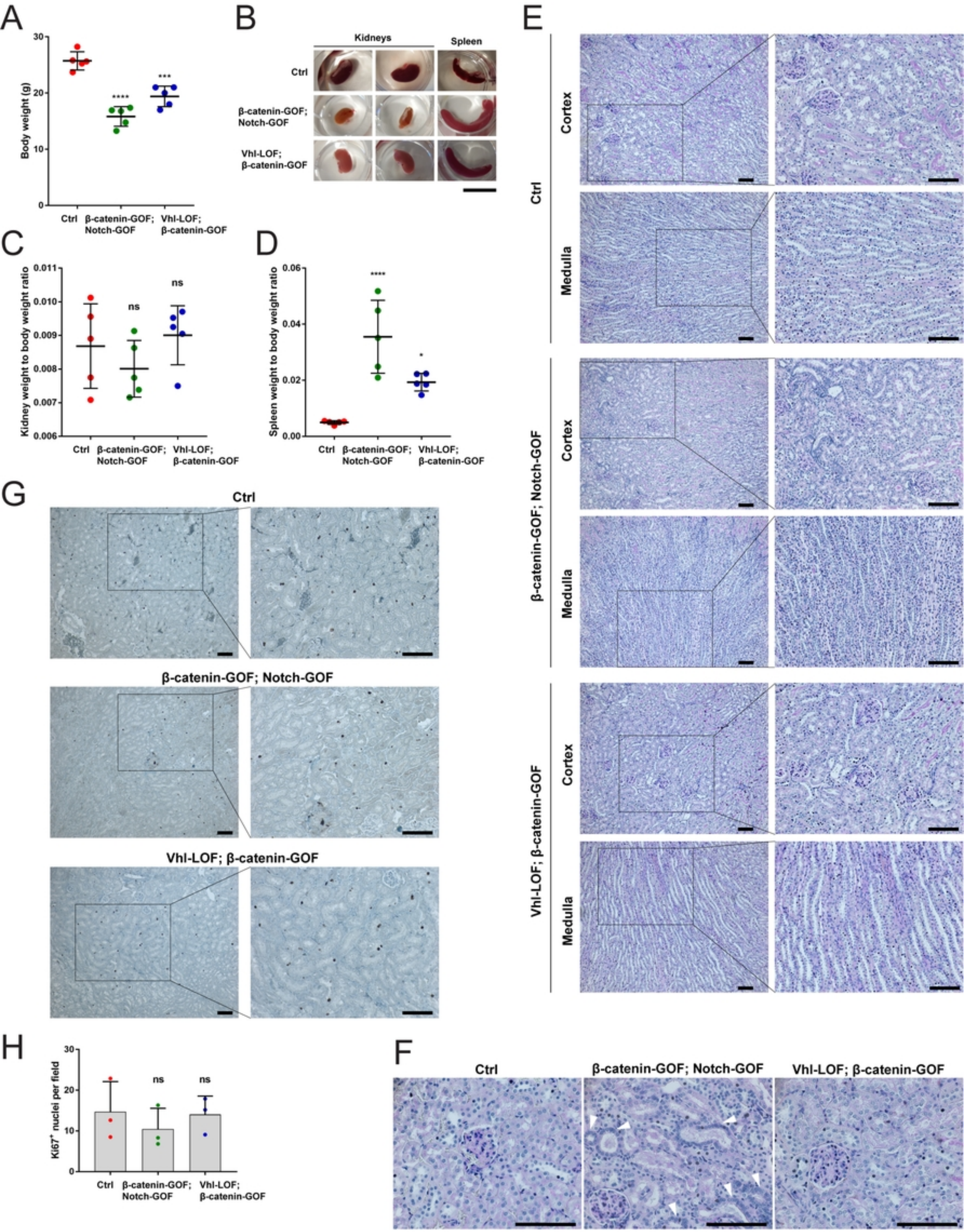
A
Body weight (g)
30
20
10
0
****
***
Ctrl
β-catenin-GOF; Notch-GOF
Vhl-LOF; β-catenin-GOF
B
Kidneys
Spleen
Ctrl
β-catenin-GOF; Notch-GOF
Vhl-LOF; β-catenin-GOF
C
Kidney weight to body weight ratio
0.011
0.010
0.009
0.008
0.007
0.006
ns
ns
Ctrl
β-catenin-GOF; Notch-GOF
Vhl-LOF; β-catenin-GOF
D
Spleen weight to body weight ratio
0.06
0.04
0.02
0.00
****
*
Ctrl
β-catenin-GOF; Notch-GOF
Vhl-LOF; β-catenin-GOF
E
Ctrl
Cortex
Medulla
β-catenin-GOF; Notch-GOF
Cortex
Medulla
Vhl-LOF; β-catenin-GOF
Cortex
Medulla
G
Ctrl
β-catenin-GOF; Notch-GOF
Vhl-LOF; β-catenin-GOF
H
Ki67+ nuclei per field
30
20
10
0
ns
ns
Ctrl
β-catenin-GOF; Notch-GOF
Vhl-LOF; β-catenin-GOF
F
Ctrl
β-catenin-GOF; Notch-GOF
Vhl-LOF; β-catenin-GOF

Fig 6

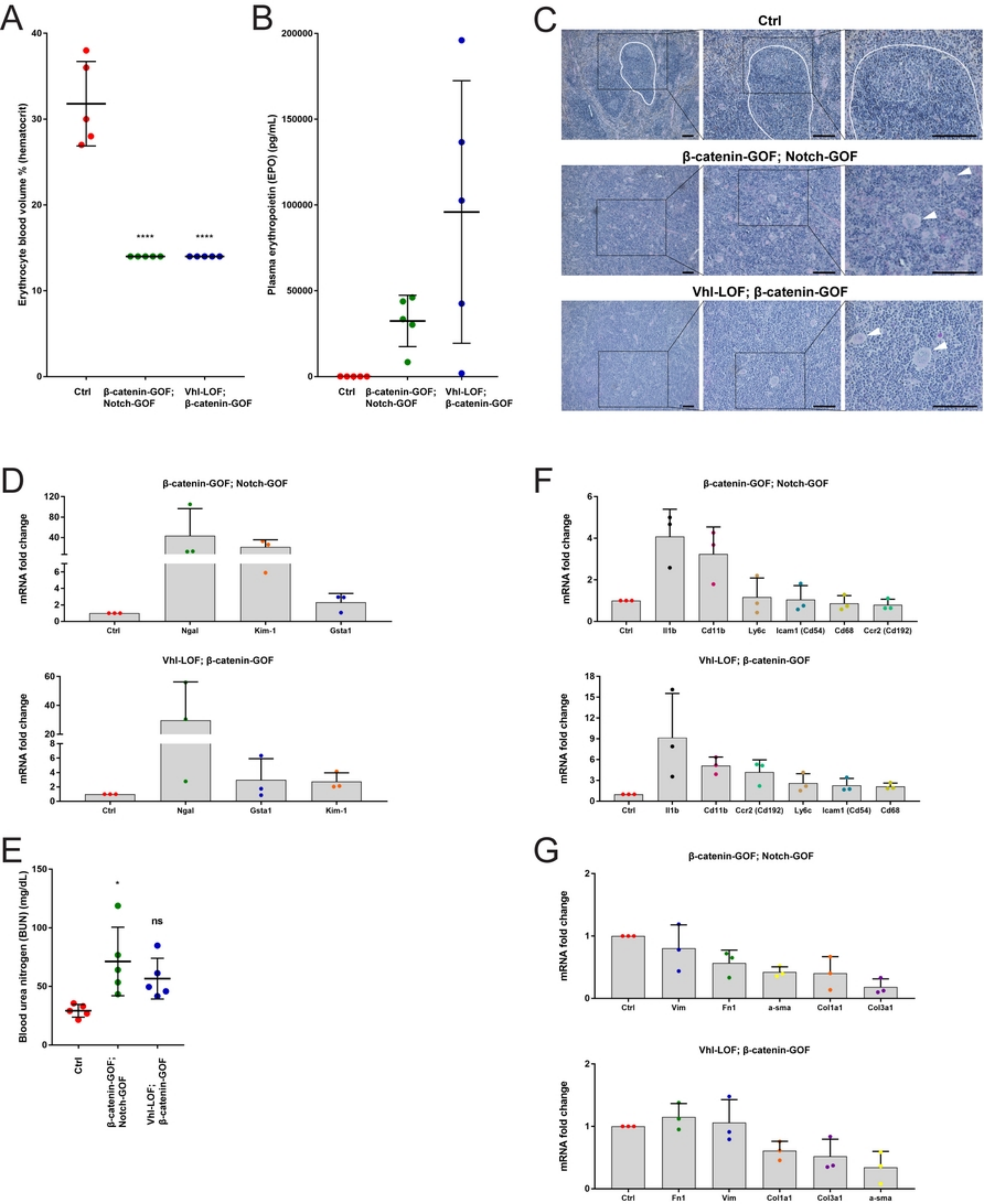
A
Erythrocyte blood volume % (hematocrit)
****
****
Ctrl
β-catenin-GOF; Notch-GOF
Vhl-LOF; β-catenin-GOF
B
Plasma erythropoietin (EPO) (pg/mL)
Ctrl
β-catenin-GOF; Notch-GOF
Vhl-LOF; β-catenin-GOF
C
Ctrl
β-catenin-GOF; Notch-GOF
Vhl-LOF; β-catenin-GOF
D
β-catenin-GOF; Notch-GOF
mRNA fold change
Ngal
Kim-1
Gsta1
Vhl-LOF; β-catenin-GOF
E
Blood urea nitrogen (BUN) (mg/dL)
*
ns
F
β-catenin-GOF; Notch-GOF
Il1b
Cd11b
Ly6c
Icam1 (Cd54)
Cd68
Ccr2 (Cd192)
Vhl-LOF; β-catenin-GOF
G
β-catenin-GOF; Notch-GOF
Vim
Fn1
a-sma
Col1a1
Col3a1
Vhl-LOF; β-catenin-GOF

Fig 7